OXFORD UNIVERSITY PRESS | Brain

NAD(P)HX Dehydratase (NAXD) deficiency: a novel neurodegenerative disorder exacerbated by febrile illnesses.

Journal:	*Brain*
Manuscript ID	BRAIN-2018-00977.R1
Manuscript Type:	Original Article
Date Submitted by the Author:	n/a
Complete List of Authors:	Van Bergen, Nicole; Murdoch Children's Research Institute, Neurodevelopmental Genomics; University of Melbourne, Paediatrics Guo, Yiran; CHOP, Department of Pediatrics Rankin, Julia; University of Exeter Medical School; Royal Devon and Exeter NHS Foundation Trust Paczia, Nicole; University of Luxembourg, Luxembourg Centre for Systems Biomedicine Becker-Kettern , Julia; University of Luxembourg, Luxembourg Centre for Systems Biomedicine Kremer, Laura; Technische Universität München, Institute of Human Genetics; Institute of Human Genetics, Helmholtz Zentrum München Pyle, Angela; Newcastle University, Wellcome Centre for Mitochondrial Research, Institute of Neuroscience, The Medical School Conrotte, Jean-François; University of Luxembourg, Luxembourg Centre for Systems Biomedicine Ellaway, Carolyn; Children's Hospital at Westmead, Western Sydney Genetics Program ; University of Sydney, Discipline of Genetic medicine; Children's Hospital at Westmead, Neurology Department Procopis, Peter; University of Sydney, Discipline of Child and Adolescent Health; Children's Hospital at Westmead, Neurology Department Prelog, Kristina; the Children's Hospital Westmead, Medical Imaging Department Homfray, Tessa; Royal Brompton and St George's University Hospital Baptista, Júlia ; University of Exeter Medical School; Royal Devon and Exeter NHS Foundation Trust Baple, Emma; University of Exeter Medical School; Royal Devon and Exeter NHS Foundation Trust Wakeling, Matthew; University of Exeter Medical School Massey, Sean; Murdoch Children's Research Institute, Neurodevelopmental Genomics Kay, Daniel; University of Luxembourg, Luxembourg Centre for Systems Biomedicine Shukla, Anju; Kasturba Medical College and Hospital, Department of Medical Genetics Girisha, Katta; Kasturba Medical College and Hospital, Department of Medical Genetics

	Lewis, Leslie; Kasturba Medical College and Hospital, Manipal Academy of Higher Education, Department of Paediatrics Santra, Saikat; Birmingham Children's Hospital Power, Rachel; Royal Brompton Hospital Daubeney, Piers; Royal Brompton Hospital; Imperial College, National Heart and Lung Institute Montoya, Julio; Universidad Zaragoza, CIBER de Enfermedades Raras (CIBERER)-Instituto de Investigación Sanitaria de Aragón (IISAragon), Departamento de Bioquimica y Biologia Molecular y Celular Ruiz-Pesini, Eduardo; Universidad de Zaragoza, Kovacs-Nagy, Reka; Institute of Human Genetics, Technische Universität München; Semmelweis University, Department of Medical Chemistry, Molecular Biology and Pathobiochemistry Pritsch, Martin ; DRK-Childrens-Hospital, Department of Pediatric Neurology Ahting, Uwe; Institute of Human Genetics, Technische Universität München Thorburn, David; Murdoch Childrens Research Institute; University of Melbourne, Department of Paediatrics; Royal Childrens Hospital, Victorian Clinical Genetics Services Prokisch, Holger; Helmholtz Zentrum, Institute of Human Genetics; Institute of Human Genetics, Technische Universität München Taylor, Robert; Newcastle University, Wellcome Centre for Mitochondrial Research, Institute of Neuroscience, The Medical School Christodoulou, John; Murdoch Childrens Research Institute, Neurodevelopment Genomics Research Group; University of Melbourne, Department of Paediatrics; Children's Hospital at Westmead, Western Sydney Genetics Program ; Royal Childrens Hospital, Victorian Clinical Genetics Services Linster, Carole ; University of Luxembourg, Luxembourg Centre for Systems Biomedicine Ellard, Sian; University of Exeter Medical School; Department of Molecular Genetics, Royal Devon and Exeter NHS Foundation Trust Hakonarson, Hakon; The Children's Hospital of Philadelphia, Perelman School of Medicine, University of Pennsylvania, Center for Applied Genomics
Subject category:	Genetics
To search keyword list, use whole or part words followed by an *:	Mitochondrial diseases < GENETICS, NEURODEGENERATION: CELLULAR AND MOLECULAR, Genetics: neurodegeneration < GENETICS, Whole-exome sequencing < GENETICS, Whole-genome sequencing < GENETICS

Title

NAD(P)HX Dehydratase (NAXD) deficiency: a novel neurodegenerative disorder exacerbated by febrile illnesses.

Running title

NAXD deficiency: fever-induced neurodegeneration

Author list

Nicole J Van Bergen [1,2 #], Yiran Guo [3 #], Julia Rankin [4,5 #], Nicole Paczia [6 #], Julia Becker-Kettern [6 #], Laura S Kremer [7,8], Angela Pyle [9], Jean-François Conrotte [6], Carolyn Ellaway [10, 11, 12], Peter Procopis [12, 13], Kristina Prelog [14], Tessa Homfray [15], Júlia Baptista [4,5], Emma Baple [4,5], Matthew Wakeling [4], Sean Massey[1], Daniel P Kay [6], Anju Shukla [16], Katta M Girisha [16], Leslie E. S. Lewis[17], Saikat Santra [18], Rachel Power[19], Piers Daubeney[19,20], Julio Montoya [21], Eduardo Ruiz-Pesini [21], Reka Kovacs-Nagy [7,22], Martin Pritsch [23], Uwe Ahting [7], David R Thorburn [1,2, 24], Holger Prokisch [7, 8], Robert W Taylor [9], John Christodoulou [1, 2, 10, 11, 24*], Carole L Linster [6 *], Sian Ellard [4,5 *], Hakon Hakonarson [3*].

Affiliations

[1]Murdoch Children's Research Institute, Royal Children's Hospital, Parkville, Melbourne, Australia 3052

[2]Department of Paediatrics, University of Melbourne, Parkville, Melbourne, Australia, 3052

[3]Center for Applied Genomics, Children's Hospital of Philadelphia, Philadelphia, PA 19104, USA

[4]University of Exeter Medical School, Exeter, EX4 4QD, United Kingdom

[5]Royal Devon Exeter NHS Foundation Trust, Exeter, EX4 4QD, United Kingdom

[6]Luxembourg Centre for Systems Biomedicine, University of Luxembourg, Belvaux, L-4367, Luxembourg

[7] Institute of Human Genetics, Technische Universität München, Munich, 81675, Germany

[8] Institute of Human Genetics, Helmholtz Zentrum München, Munich, 81675, Germany

[9]Wellcome Centre for Mitochondrial Research, Institute of Neuroscience, The Medical School, Newcastle University, Newcastle upon Tyne, NE2 4HH, United Kingdom

[10]Western Sydney Genetics Program, Children's Hospital at Westmead, Sydney, 2145, Australia

[11]Discipline of Genetic Medicine, University of Sydney, 2145, Sydney, Australia

[12]Neurology Department, Children's Hospital at Westmead, Sydney, 2145, Australia

[13]Discipline of Child and Adolescent Health, University of Sydney, 2145, Australia

[14]Medical Imaging Department, Children's Hospital at Westmead, Sydney, 2145, Australia
[15] Royal Brompton and St George's University Hospital, London, SW17 0RE, United Kingdom
[16] Department of Medical Genetics, Kasturba Medical College and Hospital, Manipal Academy of Higher Education, Manipal, 576104, India
[17] Department of Paediatrics, Kasturba Medical College and Hospital, Manipal Academy of Higher Education, Manipal, 576104, India
[18]Birmingham Children's Hospital, Birmingham, B4 6NH, United Kingdom
[19]Royal Brompton Hospital, London, SW3 6NP, United Kingdom
[20]National Heart and Lung Institute, Imperial College, London, SW3 6LY, United Kingdom
[21]Departamento de Bioquimica y Biologia Molecular y Celular- CIBER de Enfermedades Raras (CIBERER)-Instituto de Investigación Sanitaria de Aragón (IISAragon), Universidad Zaragoza, Zaragoza, 50013, Spain
[22]Department of Medical Chemistry, Molecular Biology and Pathobiochemistry, Semmelweis University, Budapest, 1085, Hungary
[23]Department of Pediatric Neurology, DRK-Childrens-Hospital, Siegen, 57072, Germany
[24]Victorian Clinical Genetics Services, Royal Children's Hospital, Melbourne, 3052, Australia

# These authors contributed equally to the work; * Equally contributing senior authors.

Corresponding authors

Correspondence to: Professor John Christodoulou, Neurodevelopmental Genomics Research Group, Murdoch Childrens Research Institute, 50 Flemington Rd Parkville, 3052, Victoria, Australia. Phone: +61 3 9936 6516, Fax: + 61 3 9348 1391
E-mail: john.christodoulou@mcri.edu.au
Correspondance to: Dr. Carole L Linster, Luxembourg Centre for Systems Biomedicine (LCSB), Université du Luxembourg, Campus Belval, 6, avenue du Swing, L-4367 Belvaux, Luxembourg. Phone: +352 466644 6231 Fax: +352 466644 36231
E-mail: carole.linster@uni.lu

Conflicts of Interest

All authors declare that they have no conflict of interest.

67

68 **Author contributions**

69 Conceived and designed the experiments: NVB, YG, JR, NP, JBK, JFC, LSK, SM, DPK, HP,
70 JC, CLL, SE.

71 Performed the experiments: NVB, YG, JR, NP, JBK, JFC, LSK, SM, DPK, MW

72 Provided clinical details of the patients: JR, LK, CE, PP, KP, TH, JB, EB, AS, KG, LL, SS,
73 RP, PD, JM, RK, HP, RWT, JC, SE.

74 Analyzed the data: NVB, YG, JR, NP, JBK, LSK, AP, JFC, LK, SM, DPK, CLL, EB, JB, SE

75 Wrote the manuscript: NVB, NP, JBK, JC, CLL.

76 Reviewed the manuscript: NVB, YG, JR, NP, JBK, LSK, AP, JFC, CE, PP, KP, TH, JB, EB,
77 MW, GJ, SM, DPK, AS, KMG, LESL, SS, RP, PD, JM, RKN, MP, DT, HP, RWT, JC, CLL,
78 SE, HH.

Abstract

Physical stress, including high temperatures, may damage the central metabolic nicotinamide nucleotide cofactors (NAD(P)H), generating toxic derivatives (NAD(P)HX). The highly conserved enzyme NAD(P)HX Dehydratase (NAXD) is essential for intracellular repair of NAD(P)HX. Here we present a series of infants and children who suffered episodes of febrile illness-induced neurodegeneration or cardiac failure and early death. Whole exome sequencing or Whole genome sequencing identified recessive *NAXD* variants in each case. Variants were predicted to be potentially deleterious through *in silico* analysis. Reverse-transcription PCR confirmed altered splicing in one case. Subject fibroblasts showed highly elevated concentrations of the damaged cofactors S-NADHX, R-NADHX and cyclic NADHX. NADHX accumulation was abrogated by lentiviral transduction of subject cells with wild-type *NAXD*. Subject fibroblasts and muscle biopsies showed impaired mitochondrial function, higher sensitivity to metabolic stress in media containing galactose and azide but not glucose, and decreased mitochondrial ROS production. Recombinant NAXD protein harbouring two missense variants leading to the amino acid changes p.(Gly63Ser) and p.(Arg608Cys) were thermolabile and showed a decrease in Vmax and increase in Km for the ATP-dependent NADHX dehydratase activity. This is the first study to identify pathogenic variants in *NAXD* and to link deficient NADHX repair with mitochondrial dysfunction. The results show that NAXD deficiency can be classified as a metabolite repair disorder in which accumulation of damaged metabolites likely triggers devastating effects in tissues such as the brain and the heart, eventually leading to early childhood death.

Key words

Metabolite repair
Mitochondria
Febrile illness
Dehydratase
Epimerase

Abbreviations

AA	amino acid
ACMG	American College of Medical Genetics
AR	autosomal recessive
ATP5A	ATP synthase subunit alpha
CXH	cycloheximide
CMV	Cytomegalovirus
COX2	cytochrome c oxidase subunit 2
CSF	Cerebrospinal fluid
CT	computed tomography
DHE	dihydroethidium
DMEM	Dulbecco's Modified Eagle's Medium
EBV	Epstein–Barr virus
ECMO	extracorporeal membrane oxygenation
EEG	electroencephalography
EST	expressed sequence tags
FBS	fetal bovine serum
GAPDH	glyceraldehyde 3-phosphate dehydrogenase
Het	heterozygous
Hom	homozygous
HRAM RP-LC-MS mass spectrometry	high resolution accurate mass reversed phase liquid chromatography
IGV	Integrative Genomics Viewer
MAF	minor allele frequency
MRI	Magnetic Resonance Imaging

133	MRS	Magnetic Resonance (MR) spectroscopy
134	MWCO	molecular weight cutoff
135	NAD	nicotinamide adenine dinucleotide
136	NADP	nicotinamide adenine dinucleotide phosphate
137	NAXD	NAD(P)HX dehydratase
138	NAXE	NAD(P)HX epimerase
139	NDUFB8	NADH:Ubiquinone Oxidoreductase Subunit B8
140	OXPHOS	oxidative phosphorylation
141	PET	positron emission tomography
142	PMSF	phenylmethylsulfonyl fluoride
143	RIPA	Radioimmunoprecipitation assay buffer
144	RFU	relative fluorescent units
145	RT-PCR	Reverse-transcription PCR
146	SDHB	succinate dehydrogenase [ubiquinone] flavoprotein subunit B
147	SDS-PAGE	sodium dodecyl sulfate polyacrylamide gel electrophoresis
148	SNV	single nucleotide variant
149	UQCRC2	cytochrome b-c1 complex subunit 2
150	VCF	Variant Call Format
151	WES	whole exome sequencing
152	WGS	whole genome sequencing
153	WT	wild-type

154

Main text

Metabolism is traditionally viewed as an efficient and precise system, supported by enzymes that are highly specific for their substrate and the type of reaction through which they convert the substrate. This view has been challenged over recent years by the identification of a growing list of enzymes that function to repair or remove metabolic side products, the latter of which are generated by side reactions of main metabolic enzymes. Metabolic side products can also be produced intracellularly by unwanted spontaneous chemical reactions. These non-canonical or 'damaged' metabolites can inhibit key metabolic reactions if they are left to accumulate. It is to precisely prevent the accumulation of potentially toxic small molecules that all organisms of all domains of life have most likely evolved a panoply of metabolite repair systems (Linster *et al.*, 2013; Van Schaftingen *et al.*, 2013).

The nicotinamide nucleotides NAD (reduced form NADH, oxidized form NAD+) and NADP (reduced form NADPH, oxidized form NADP+) have essential roles in many cellular functions. NAD is involved in a series of catabolic reactions and in mitochondrial energy production, whereas NADP is a key component of numerous biosynthetic processes as well as cellular antioxidant protection systems (Ying, 2008; Houtkooper *et al.*, 2010). The nicotinamide ring within these cofactors is prone to hydration, forming NADHX or NADPHX, which can be present as *R* or *S* epimers and which can further degrade irreversibly to cyclic NAD(P)HX (Yoshida and Dave, 1975). NADHX can be slowly produced from NADH by GAPDH (Rafter *et al.*, 1954); NAD(P)HX can also form spontaneously from the normal reduced cofactors under 'stress' conditions such as increased temperature or acidic pH (Rafter *et al.*, 1954; Yoshida and Dave, 1975). The damaged cofactors cannot act as electron carriers and have been shown *in vitro* to inhibit several key dehydrogenase enzymes (Yoshida and Dave, 1975; Prabhakar *et al.*, 1998). In *Saccharomyces cerevisiae*, *in vitro* and *in vivo* evidence for an inhibitory effect of NADHX on 3-phosphoglycerate oxidoreductase, catalyzing the initial step of the serine biosynthesis pathway, has been obtained recently (Becker-Kettern *et al.*, 2018). Therefore, NAD(P)HX can be expected to be toxic to cells, and detoxification by a metabolite repair system is critical.

The nicotinamide nucleotide repair system consists of two partner enzymes: NAD(P)HX epimerase (NAXE, formerly APOA1BP; OMIM: 608862), which converts R-NAD(P)HX to S-NAD(P)HX, and NAD(P)HX dehydratase (NAXD, formerly CARKD; OMIM: 615910), which converts S-NAD(P)HX back to NAD(P)H in an ATP-dependent manner (Marbaix *et al.*, 2011). Both these enzymes are targeted to several subcellular compartments, including

the mitochondrion (Marbaix *et al.*, 2014). They also have a ubiquitous tissue distribution (Marbaix *et al.*, 2014) and are conserved across all taxa (Marbaix *et al.*, 2011). The presence of the NAD(P)HX repair enzymes across all tissues and species, combined with the central metabolic roles of the cofactors that they function to preserve, suggest that the repair system is critical to sustain life. More specifically, it can be predicted that the brain, which has a very high and constant demand for energy supply generated by mitochondria, would be particularly vulnerable to impaired NAD(P)HX repair and as such, the NAXE and NAXD enzymes would be critical to support normal brain function. In apparent contradiction with those predictions, however, knocking out NAD(P)HX repair enzymes in other organisms such as yeast, bacteria and plants, has so far only revealed subtle growth phenotypes, if any, at least under standard growth conditions (Breslow *et al.*, 2008; Hillenmeyer *et al.*, 2008; Nichols *et al.*, 2011; Colinas *et al.*, 2014; Niehaus *et al.*, 2014; Becker-Kettern *et al.*, 2018).

Recently whole exome sequencing (WES) identified pathogenic variants in the epimerase *NAXE* that were associated with cases of a lethal neurometabolic disorder of early childhood (Kremer *et al.*, 2016; Spiegel *et al.*, 2016). In these subjects, it appeared that episodes of febrile illness aggravated the consequences of an already compromised metabolite repair system, resulting in rapid neurological deterioration and decomposition of other tissues with clinical observation of ataxia, muscular hypotonia, respiratory insufficiency and/or respiratory failure, nystagmus and skin manifestations followed by premature death. This provided the first cases of subjects with pathogenic variants in a key enzyme of the nicotinamide nucleotide repair pathway.

In the present study we report six unrelated individuals with homozygous or compound heterozygous variants in *NAXD*. The predominant clinical features included repeated episodes of regression often triggered by episodes of mild fever or infection, an infantile onset neurodegenerative condition (Figure 1 A - M) and skin lesions (Figure O – P), ultimately leading to early death in all cases. The clinical features of our NAXD subjects therefore resembled those of the previously published cases of NAXE deficiency (Table 1), and detailed clinical reports for all cases are available in Supplementary Materials. The six subjects with *NAXD* variants were identified individually by WES or WGS as part of either independent international gene discovery cohorts, National Health Services diagnostic testing or through the Genematcher/Matchmaker database (Philippakis *et al.*, 2015; Sobreira *et al.*, 2015).

Sanger sequencing confirmed all variants identified through next generation sequencing (Supplementary Fig. 1). The human *NAXD* gene is predicted to generate four coding

transcripts, leading to the expression of cytosolic, mitochondrial and ER protein isoforms, as explained in detail in Supplemental Material (see also Supplementary Figs. 2 and 3). For initial interpretation we focused on the most abundant transcript RefSeq isoform c (NM_001242882.1; Supplementary Table 1) whose existence is most strongly supported by EST analysis and from which mitochondrial and cytosolic NAXD protein forms can be translated (as described in Supplemental Material). *In silico* analyses predicted the variants to be pathogenic to each of the four *NAXD* transcript isoforms (NCBI RefSeq), and affect the structure and function of the NAXD protein (Supplementary Table 2, Supplementary Fig. 2 and Supplementary Fig. 3). By HSF3 analysis (Desmet *et al.*, 2009) the splicing variant in Case 1 was predicted to lead to disruption of the wild-type donor site, which was confirmed by RT-PCR studies, revealing aberrant splicing and skipping of Exon 9 (Supplementary Fig. 4).

We then used patient fibroblasts to determine the intracellular concentrations of NAD(P), NAD(P)H, S-NAD(P)HX, R-NAD(P)HX and cyclic-NAD(P)HX using high resolution accurate mass reversed phase liquid chromatography mass spectrometry (HRAM RP-LC-MS) with comparison against chemically pure standards (Supplementary Fig. 5). We detected no significant differences in NAD, NADH and NADP levels between control and subject-derived fibroblasts (NADPH levels were below the limit of quantification). Importantly, the damaged cofactor derivatives S-NADHX, R-NADHX and cyclic-NADHX were only detected in fibroblasts from Cases 1, 2 and 4, but not in any of our control cell lines (Fig. 2A and B). Quantification of these metabolites revealed a similar level of accumulation of S-NADHX and R-NADHX in Case 1, Case 2 and Case 4 (Fig. 2C). Interestingly the levels detected in Case 3 were much lower than for Cases 1, 2 and 4 and only just above the detection threshold for LC-MS analysis (Figure 2B). Lentiviral transduction with either the cytosolic (cNAXD) or mitochondrial (mNAXD) wild-type *NAXD* cDNA completely prevented the accumulation of any of the NADHX derivatives in fibroblasts from Case 1 and 2 (Fig. 2D) whilst a control GFP construct had no effect (Fig. 2D).

To address whether mitochondrial function is affected by NAXD deficiency in our subjects, we examined the expression of representative protein subunits of the mitochondrial respiratory chain and enzyme activity of Complex I and Complex IV in fibroblasts from Case 1 and 2. There was a marked reduction in the expression of both NDUFB8 (Complex I membrane subunit) and COXII (Complex IV subunit) in both Case 1 and Case 2 compared to four pediatric control fibroblast extracts (Fig. 3A and Supplementary Fig. 6). We found a significant reduction in cytochrome *C* oxidase activity in Case 1 and Case 2 compared to

controls (Fig. 3B), whilst Complex I NADH oxidation activity was not affected (data not shown). Mitochondrial superoxide production revealed a significant decrease in rotenone-inhibited complex I superoxide production in both Case 1 and Case 2 compared to controls (Fig. 3C). There was a significant decrease in the growth rate of fibroblasts in basal media or in glucose-free, galactose-azide medium to induce mitochondrial stress from Case 1 and Case 2 compared to control fibroblasts (Fig. 3D).

The *NAXD* missense variants (p.(Arg308Cys) and p.(Gly63Ser)) were introduced by site-directed mutagenesis into human *NAXD* cDNA, then expressed and purified as recombinant proteins. For the p.(Gly63Ser) variant, we found a 3.4-fold decrease in Vmax and a 3.3-fold increase in Km compared to the wild-type protein. For the p.(Arg308Cys) variant, we determined a 2.5-fold decrease in Vmax and a 2.2-fold increase in Km compared to wild-type (Supplementary Table 3). Thermostability analyses of recombinant NAXD revealed that both the p.(Gly63Ser) and the p.(Arg308Cys) proteins lost enzymatic activity upon pre-incubation at temperatures higher than 30°C while the wild-type protein activity resisted exposure to temperatures up to 47°C (Fig. 3E). This thermolability was most pronounced for the p.(Arg308Cys) variant, with a more than 90% decrease in activity above 45ºC, while for the p.(Gly63Ser) variant this same treatment resulted in an ~ 40% activity loss (Fig. 3E).

Here we report on the first known pathogenic *NAXD* variants, which affected six families, leading to a fever-induced severe multisystem disease and death within the first decade of life. To explore the consequences of NAXD deficiency, quantification of NAD(P)HX metabolites revealed a similar level of accumulation of S-NADHX and R-NADHX in Case 1, Case 2 and Case 4 in the expected 60:40 S to R epimer ratio (Marbaix *et al.*, 2011). This was completely reversed by lentiviral transduction with either cytosolic (cNAXD) or mitochondrial (mNAXD) lentiviral constructs. Supposing an intracellular fibroblast volume of 2 picoliters, the approximate intracellular concentrations of S-NADHX (100 – 300 µM) and R-NADHX (70 – 210 µM) were quantitatively similar to values induced by a complete loss of function for NAXD in an experimental cell line (Becker-Kettern *et al.*, 2018). The levels in Case 3 were only just above the detection threshold which may be due to the frameshift mutation in this patient preventing expression of the mitochondrial and ER targeted NAXD isoforms (early truncation), but allowing for expression of the cytosolic NAXD protein from the ATG residing in exon 2 (Met3 in Supplementary Fig. 3). The same reasoning would also apply to Case 5, for which fibroblasts were, however, not available for measurements. These results provide strong support that the NADHX accumulation is specifically caused by *NAXD* mutations.

NAD(P)H are essential cofactors for many cellular reactions, particularly in the mitochondria, therfore accumulation of the non-canonical NAD(P)HX derivatives may impede multiple cellular functions including key mitochondrial dehydrogenases (Yoshida and Dave, 1975; Prabhakar *et al.*, 1998). Subjects with pathogenic variants in *NAXE* had decreased complex I activity (Kremer *et al.*, 2016) indicating impaired mitochondrial function as a consequence of a deficiency in one of the NAD(P)HX repair enzymes. Respiratory chain activity was impaired in NAXD patients; fibroblasts had a significant decrease in the expression of complex I and IV, and activity of complex IV and muscle enzymology showed reduced respiratory chain activity (Complex II+III, Case 2; Complex I, Case 4; Complex I and IV, Case 6). We also demonstrated reduced superoxide production in NAXD subjects, which may be explained by decreased expression of specific Complex I subunits subsequently affecting holocomplex stability, but partial enzyme activity may still remain due to preservation of NADH oxidation in the matrix arm of Complex I. Mitochondrial dysfunction can also be revealed by culturing cells under galactose growth conditions (Robinson *et al.*, 1992) in the presense of the Complex IV inhibitor sodium azide (Swalwell *et al.*, 2011), which limits ATP production by glycolysis, forcing cells to rely on mitochondrial OXPHOS. There was a significant decrease in the growth rate of fibroblasts from Case 1 and Case 2 compared to control fibroblasts under galactose conditions, further supporting that mitochondrial function in fibroblasts from NAXD subjects is compromised.

To determine the effect of the *NAXD* missense variants (p.(Arg308Cys) and p.(Gly63Ser)) on NADHX dehydratase activity, the missense variants were introduced by site-directed mutagenesis into the cytosolic *NAXD* cDNA since similar kinetic properties were previously obtained for both mitochondrial and cytosolic Carkd (mouse homologue of human NAXD) (Marbaix *et al.*, 2011) and the cytosolic protein gave greater yield. Analysis of the kinetic properties for the two missense variants revealed significantly reduced Vmax and increased Km compared to the wild-type protein. Thermostability analysis revealed loss of enzymatic activity upon pre-incubation temperatures above 30°C, and the thermolability was more pronounced for the p.(Arg308Cys) variant. The Gly63 residue is highly conserved from bacteria to humans (Marbaix *et al.*, 2011); the Arg308 residue is also conserved in the mouse and yeast homologs of *NAXD*, but not in the *E. coli* homolog (Marbaix *et al.*, 2011). This arginyl residue is relatively close to the C-terminus of the protein, as are the splicing and frameshift mutations found in Case 1 and Case 2, respectively, suggesting that this may be a critical domain for NAXD protein stability. In addition, the thermolability of the NAXD missense variants found in Case 1 and Case 2 may at least in part explain the coincidence of

deterioration in the subjects sometimes occurring after episodes of fever. Those individuals who had infections may have had unreported fevers secondary to the viral infection which likely precipitated rapid decompensation. In summary, our *in vitro* analyses of recombinant NAXD demonstrated that the missense variants, while retaining residual enzyme activity, show a markedly decreased stability especially at higher temperatures.

This report highlights the importance of the NAD(P)HX repair system to preserve cellular and overall health in humans. We could show high intracellular NADHX accumulation for three of the four individuals where fibroblast lines were available for analysis, and impaired mitochondrial function. The missense variants found in Case 1 and Case 2 led to partial loss of enzyme activity and a significant decrease in thermostability. More particularly, NAXD deficiency appears to have devastating effects in key tissues such as the brain, which are critically dependent on efficient energy metabolism and are exquisitely sensitive to abnormal metabolite accumulation. After 2-hydroxyglutaric aciduria (Van Schaftingen *et al.*, 2009) and NAXE deficiency (Kremer *et al.*, 2016), NAXD deficiency represents now the third known disorder of metabolite repair. We also suggest that NAXD deficiency should be included in the growing list of genetic disorders associated with fever-induced neurological deterioration (Powers and Scheld, 1996; Longo, 2003).

Acknowledgements

We thank the families for their support.

Funding

We thank the Crane and Perkins families and the Lions International Club Esch-sur-Alzette for donations to this research. The research conducted at the Murdoch Children's Research Institute was supported by the Victorian Government's Operational Infrastructure Support Program. JBK and NP were supported by an AFR-PhD grant (4044610) and a CORE junior grant (C16/BM/11339953), respectively, of the Fonds National de la Recherche Luxembourg. Sequencing, data analysis and Sanger validation of one sample (Case 1) were done in the Center for Applied Genomics at the Children's Hospital of Philadelphia through research funding from Aevi Genomic Medicine Inc. This study was partly supported by the German Bundesministerium für Bildung und Forschung (BMBF) through the German Network for mitochondrial disorders (mitoNET, 01GM1113 for HP) and through the E-Rare project GENOMIT (01GM1603 for HP). HP is supported by EU Horizon2020 Collaborative

Research Project SOUND (633974). This work was supported by grants from Instituto de Salud Carlos III (PI17/00021); Departamento de Ciencia, Tecnología y Universidad del Gobierno de Aragón (Grupos de Referencia B33_17R). RWT is supported by the Wellcome Centre for Mitochondrial Research (203105/Z/16/Z), the Medical Research Council (MRC) Centre for Translational Research in Neuromuscular Disease and Mitochondrial Disease Patient Cohort (UK) (G0800674), the Lily Foundation and the UK NHS Highly Specialised Service for Rare Mitochondrial Disorders of Adults and Children. SE is a Wellcome Trust Senior Investigator. The authors declare no competing financial interests.

Supplementary Material

Supplementary material contains full *in silico* analysis of *NAXD* variants, primer sequences, enzyme kinetic data, NAXD protein sequence alignment, Sanger confirmation, splice analysis, NADHX isotope distribution, representative western blots all materials and methods, NAXD transcript analysis and full clinical reports for all cases.

Fig. and Table Legends

Table 1: Clinical findings in individuals with variants in *NAXD* or *NAXE*

* abnormal MRI scan; ^ one episode of fever without any deterioration; # sibling had mild developmental delay, mild anemia, recurrent episodes of fever, and died after an episode of vomiting and lethargy at 1 year 7 months.

Fig. 1 – Neuroimaging findings and skin manifestations in children with *NAXD* mutations

MRI scans for Case 1 at the age of 3 years and 7 months, three months after normal MRI scans (A; Axial T2, B; Diffusion (DWI) and C; coronal T2 FLAIR) showed bilateral and symmetrical T2 high signal and cytotoxic oedema of the basal ganglia and focal areas of cortical involvement in the temporal lobes. Progress MRI after 3 weeks (D; axial T2, E; DWI and F; coronal T2 FLAIR) showed bilateral and symmetrical T2 high signal and cytotoxic oedema of the basal ganglia persist with increasing areas of asymmetrical cortical involvement in the temporal lobes and frontal lobes. Follow-up MRI 3 years later (G; Axial T2, H; axial and I; coronal T2 FLAIR) showed generalised cerebral atrophy, most marked in the frontal lobes and basal ganglia with exvacuo-dilatation of the lateral ventricles. The high signal is consistent with gliosis. Case 2 MRI (J – M) showed bilateral hyperintensity of striatal nuclei which remained unchanged in subsequent scans. Case 4 brain MRI (N) showed bilateral basal ganglia changes suggestive of a mitochondrial disorder. Extensive skin lesions in Case 4 (O – P).

Fig. 2: NADHX accumulation in subject fibroblasts and phenotypic rescue by lentiviral gene delivery of wild-type *NAXD*

Representative examples of LC-MS extracted ion chromatograms of A) S- and R-NADHX metabolites (XIC = 682.12) and B) NADH and cyclic NADHX (XIC = 664.11). The chromatograms clearly show peaks of S-, R- and cyclic NADHX in Case 1 and Case 2, and not in a control. C) Quantitative results of the NADHX measurements after cultivation of fibroblasts from Cases 1, 2, 3 and 4 under standard conditions at 37°C for 96 hours. Note that these metabolites were not detected in four control fibroblast lines. Data is mean +/- SD, n = 3. C) Quantitative results of the NADHX measurements in lentiviral-rescued cells. There was a clear accumulation of S-, R- and cyclic NADHX in Case 1 and Case 2, independently of

transduction with GFP-only vectors. S-, R- and cyclic NADXH were not detected in control fibroblasts. Lentiviral gene rescue with either the mNAXD or cNAXD construct completely prevented accumulation of S-, R- and cyclic NADHX in subject cells. Data is mean +/- SD, n = 3.

Fig. 3 - Mitochondrial impairment in NAXD subject fibroblasts and thermostability of recombinant NAXD protein variants

A) Mitochondrial OXPHOS proteins were separated by SDS-PAGE, probed for relative expression levels of key OXPHOS subunits by immunoblotting, and expression levels normalized to GAPDH as a loading control. There was a significant decrease in the expression of Complex I and Complex IV proteins expression in Case 1 and Case 2 compared to controls. B) Mitochondrial OXPHOS enzyme activity was measured in cell extracts by immunocapture dipstick assays. There was a significant decrease in Complex IV activity (mAbs/mg protein) in Case 1 and Case 2 relative to controls. C) Relative rates (relative fluorescent units/time) of mitochondrial superoxide production in fibroblasts was measured with the superoxide sensitive probe dihydroethidium in the presence or absence of the Complex I inhibitor rotenone. D) Growth rate in medium devoid of glucose but containing 5mM galactose and 50µM sodium azide was normalized to growth rate in basal medium to account for variation in the baseline growth rate of each cell line. The normalized growth rate in Case 1 and Case 2 was significantly lower than controls. E) Purified recombinant NAXD protein, without or with missense mutations p.(Gly63Ser) and p.(Arg308Cys), was pre-incubated at the indicated temperature for 30 min prior to addition to a reaction mixture for the spectrophotometric assay of NADHX dehydratase activity. Data is mean ± SD, n>3 per measurement from at least two independent experiments. Statistical significance was determined using one-way ANOVA with Bonferroni correction for multiple comparisons, * $P<0.05$; ** $P<0.01$; *** $P<0.001$.

References

Adzhubei IA, Schmidt S, Peshkin L, Ramensky VE, Gerasimova A, Bork P, *et al.* A method and server for predicting damaging missense mutations. Nat Methods 2010; 7(4): 248-9.

Becker-Kettern J, Paczia N, Conrotte J-F, Zhu C, Fiehn O, Jung PP, *et al.* NAD(P)HX repair deficiency causes central metabolic perturbations in yeast and human cells. bioRxiv 2018.

Breslow DK, Cameron DM, Collins SR, Schuldiner M, Stewart-Ornstein J, Newman HW, *et al.* A comprehensive strategy enabling high-resolution functional analysis of the yeast genome. Nat Methods 2008; 5(8): 711-8.

Calvo SE, Compton AG, Hershman SG, Lim SC, Lieber DS, Tucker EJ, *et al.* Molecular diagnosis of infantile mitochondrial disease with targeted next-generation sequencing. Sci Transl Med 2012; 4(118): 118ra10.

Chaykin S, Meinhart JO, Krebs EG. Isolation and properties of a reduced diphosphopyridine nucleotide derivative. J Biol Chem 1956; 220(2): 811-20.

Colinas M, Shaw HV, Loubery S, Kaufmann M, Moulin M, Fitzpatrick TB. A pathway for repair of NAD(P)H in plants. J Biol Chem 2014; 289(21): 14692-706.

Cooper GM, Stone EA, Asimenos G, Program NCS, Green ED, Batzoglou S, *et al.* Distribution and intensity of constraint in mammalian genomic sequence. Genome Res 2005; 15(7): 901-13.

Danecek P, Auton A, Abecasis G, Albers CA, Banks E, DePristo MA, *et al.* The variant call format and VCFtools. Bioinformatics 2011; 27(15): 2156-8.

Desmet FO, Hamroun D, Lalande M, Collod-Beroud G, Claustres M, Beroud C. Human Splicing Finder: an online bioinformatics tool to predict splicing signals. Nucleic Acids Res 2009; 37(9): e67.

Genomes Project C, Auton A, Brooks LD, Durbin RM, Garrison EP, Kang HM, *et al.* A global reference for human genetic variation. Nature 2015; 526(7571): 68-74.

Giordano C, Iommarini L, Giordano L, Maresca A, Pisano A, Valentino ML, *et al.* Efficient mitochondrial biogenesis drives incomplete penetrance in Leber's hereditary optic neuropathy. Brain 2014; 137(Pt 2): 335-53.

Girisha KM, Shukla A, Trujillano D, Bhavani GS, Hebbar M, Kadavigere R, *et al.* A homozygous nonsense variant in IFT52 is associated with a human skeletal ciliopathy. Clin Genet 2016; 90(6): 536-9.

Guo Y, Ding X, Shen Y, Lyon GJ, Wang K. SeqMule: automated pipeline for analysis of human exome/genome sequencing data. Sci Rep 2015; 5: 14283.

Hillenmeyer ME, Fung E, Wildenhain J, Pierce SE, Hoon S, Lee W, *et al.* The chemical genomic portrait of yeast: uncovering a phenotype for all genes. Science 2008; 320(5874): 362-5.

Houtkooper RH, Canto C, Wanders RJ, Auwerx J. The secret life of NAD+: an old metabolite controlling new metabolic signaling pathways. Endocr Rev 2010; 31(2): 194-223.

Kremer LS, Bader DM, Mertes C, Kopajtich R, Pichler G, Iuso A, *et al.* Genetic diagnosis of Mendelian disorders via RNA sequencing. Nat Commun 2017; 8: 15824.

Kremer LS, Danhauser K, Herebian D, Petkovic Ramadza D, Piekutowska-Abramczuk D, Seibt A, *et al.* NAXE Mutations Disrupt the Cellular NAD(P)HX Repair System and Cause a Lethal Neurometabolic Disorder of Early Childhood. Am J Hum Genet 2016; 99(4): 894-902.

Kumar P, Henikoff S, Ng PC. Predicting the effects of coding non-synonymous variants on protein function using the SIFT algorithm. Nat Protoc 2009; 4(7): 1073-81.

Lek M, Karczewski KJ, Minikel EV, Samocha KE, Banks E, Fennell T, *et al.* Analysis of protein-coding genetic variation in 60,706 humans. Nature 2016; 536(7616): 285-91.

Linster CL, Van Schaftingen E, Hanson AD. Metabolite damage and its repair or pre-emption. Nat Chem Biol 2013; 9(2): 72-80.

Longo N. Mitochondrial encephalopathy. Neurol Clin 2003; 21(4): 817-31.

Marbaix AY, Noel G, Detroux AM, Vertommen D, Van Schaftingen E, Linster CL. Extremely conserved ATP- or ADP-dependent enzymatic system for nicotinamide nucleotide repair. J Biol Chem 2011; 286(48): 41246-52.

Marbaix AY, Tyteca D, Niehaus TD, Hanson AD, Linster CL, Van Schaftingen E. Occurrence and subcellular distribution of the NADPHX repair system in mammals. Biochem J 2014; 460(1): 49-58.

Ng PC, Henikoff S. Predicting deleterious amino acid substitutions. Genome Res 2001; 11(5): 863-74.

Nichols RJ, Sen S, Choo YJ, Beltrao P, Zietek M, Chaba R, *et al.* Phenotypic landscape of a bacterial cell. Cell 2011; 144(1): 143-56.

Niehaus TD, Richardson LG, Gidda SK, ElBadawi-Sidhu M, Meissen JK, Mullen RT, *et al.* Plants utilize a highly conserved system for repair of NADH and NADPH hydrates. Plant Physiol 2014; 165(1): 52-61.

Philippakis AA, Azzariti DR, Beltran S, Brookes AJ, Brownstein CA, Brudno M, *et al.* The Matchmaker Exchange: a platform for rare disease gene discovery. Hum Mutat 2015; 36(10): 915-21.

Plagnol V, Curtis J, Epstein M, Mok KY, Stebbings E, Grigoriadou S, *et al.* A robust model for read count data in exome sequencing experiments and implications for copy number variant calling. Bioinformatics 2012; 28(21): 2747-54.

Powers JH, Scheld WM. Fever in neurologic diseases. Infect Dis Clin North Am 1996; 10(1): 45-66.

Prabhakar P, Laboy JI, Wang J, Budker T, Din ZZ, Chobanian M, *et al.* Effect of NADH-X on cytosolic glycerol-3-phosphate dehydrogenase. Arch Biochem Biophys 1998; 360(2): 195-205.

Rafter GW, Chaykin S, Krebs EG. The action of glyceraldehyde-3-phosphate dehydrogenase on reduced diphosphopyridine nucleotide. J Biol Chem 1954; 208(2): 799-811.

Richards S, Aziz N, Bale S, Bick D, Das S, Gastier-Foster J, *et al.* Standards and guidelines for the interpretation of sequence variants: a joint consensus recommendation of the American College of Medical Genetics and Genomics and the Association for Molecular Pathology. Genet Med 2015; 17(5): 405-24.

Robinson BH, Petrova-Benedict R, Buncic JR, Wallace DC. Nonviability of cells with oxidative defects in galactose medium: a screening test for affected patient fibroblasts. Biochem Med Metab Biol 1992; 48(2): 122-6.

Smeitink JA, Elpeleg O, Antonicka H, Diepstra H, Saada A, Smits P, *et al.* Distinct clinical phenotypes associated with a mutation in the mitochondrial translation elongation factor EFTs. Am J Hum Genet 2006; 79(5): 869-77.

Sobreira N, Schiettecatte F, Valle D, Hamosh A. GeneMatcher: a matching tool for connecting investigators with an interest in the same gene. Hum Mutat 2015; 36(10): 928-30.

Spiegel R, Shaag A, Shalev S, Elpeleg O. Homozygous mutation in the APOA1BP is associated with a lethal infantile leukoencephalopathy. Neurogenetics 2016; 17(3): 187-90.

Stenson PD, Mort M, Ball EV, Howells K, Philips AD, Thomas NS, *et al.* The Human Gene Mutation Database: 2008 update. . Genome Med 2009; 1(13).

Swalwell H, Kirby DM, Blakely EL, Mitchell A, Salemi R, Sugiana C, *et al.* Respiratory chain complex I deficiency caused by mitochondrial DNA mutations. Eur J Hum Genet 2011; 19(7): 769-75.

Valente L, Tiranti V, Marsano RM, Malfatti E, Fernandez-Vizarra E, Donnini C, *et al.* Infantile encephalopathy and defective mitochondrial DNA translation in patients with mutations of mitochondrial elongation factors EFG1 and EFTu. Am J Hum Genet 2007; 80(1): 44-58.

530 Van Schaftingen E, Rzem R, Marbaix A, Collard F, Veiga-da-Cunha M, Linster CL.
531 Metabolite proofreading, a neglected aspect of intermediary metabolism. J Inherit Metab Dis
532 2013; 36(3): 427-34.
533 Van Schaftingen E, Rzem R, Veiga-da-Cunha M. L: -2-Hydroxyglutaric aciduria, a disorder
534 of metabolite repair. J Inherit Metab Dis 2009; 32(2): 135-42.
535 Wang K, Li M, Hakonarson H. ANNOVAR: functional annotation of genetic variants from
536 high-throughput sequencing data. Nucleic Acids Res 2010; 38(16): e164.
537 Yang X, Boehm JS, Yang X, Salehi-Ashtiani K, Hao T, Shen Y*, et al.* A public genome-scale
538 lentiviral expression library of human ORFs. Nat Methods 2011; 8(8): 659-61.
539 Ying W. NAD+/NADH and NADP+/NADPH in cellular functions and cell death: regulation
540 and biological consequences. Antioxid Redox Signal 2008; 10(2): 179-206.
541 Yoshida A, Dave V. Inhibition of NADP-dependent dehydrogenases by modified products of
542 NADPH. Arch Biochem Biophys 1975; 169(1): 298-303.

Table 1: Clinical findings in individuals with variants in *NAXD* or *NAXE*

Clinical presentation	***NAXD* cases (present study)**						***NAXE* (previously published)**	
	Case 1	**Case 2**	**Case 3**	**Case 4**	**Case 5**	**Case 6**	**(Spiegel et al 2016)**	**(Kremer et al 2016)**
Gender	M	F	F	M	F	F	3F, 2M	2F, 4M
Episodes of fever/illness prior to deterioration	Y	Y δ	Y	Y	Y	Y	5/5	4/6 (2 unclear)
Neurodegeneration	Y	Y	N	Y	? *	Y	5/5	4/6 (2 unclear)
Skin lesions	Y	Y	N	Y	N	Y	Not reported	4/6
Cardiac presentation	N	N	N	N	Y	N	Not reported	2/6 ^
Early death	Y	Y	Y #	Y	Y	Y	4/5	6/6

* abnormal MRI scan; # sibling had mild developmental delay, mild anemia, recurrent episodes of fever, and died after an episode of vomiting and lethargy at 1 year 7 months. ^ two NAXE patients died from cardiovascular failure. δ Fever was associated with some, but not all episodes of deterioration.

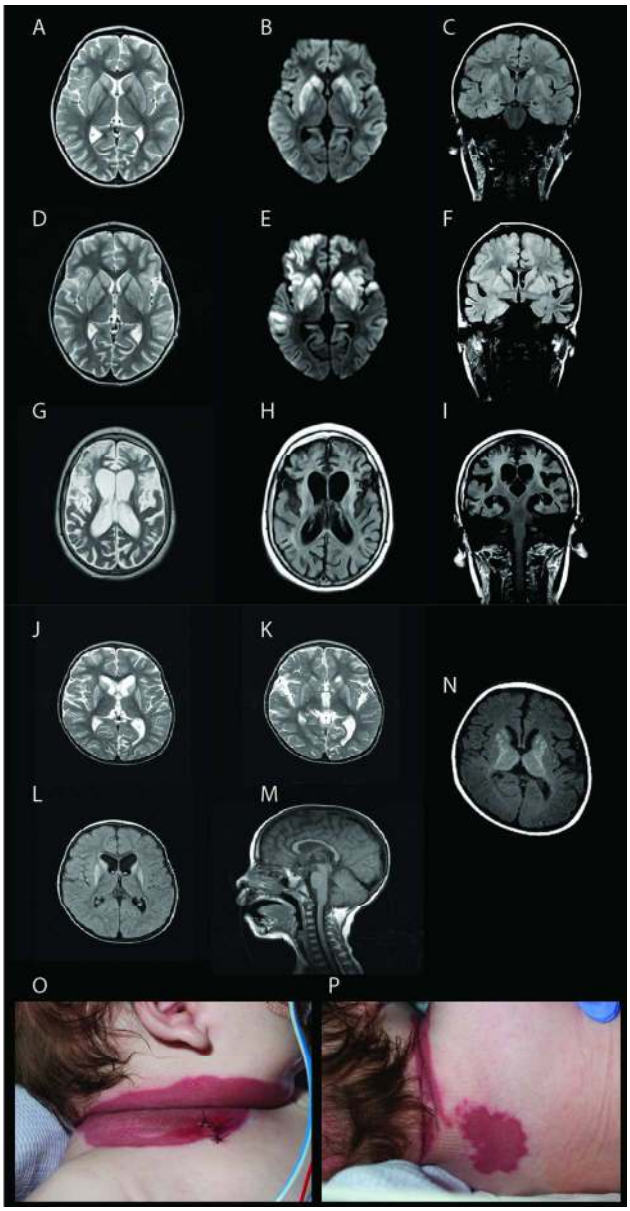

Fig. 1 – Neuroimaging findings and skin manifestations in children with NAXD mutations
MRI scans for Case 1 at the age of 3 years and 7 months, three months after normal MRI scans (A; Axial T2, B; Diffusion (DWI) and C; coronal T2 FLAIR) showed bilateral and symmetrical T2 high signal and cytotoxic oedema of the basal ganglia and focal areas of cortical involvement in the temporal lobes. Progress MRI after 3 weeks (D; axial T2, E; DWI and F; coronal T2 FLAIR) showed bilateral and symmetrical T2 high signal and cytotoxic oedema of the basal ganglia persist with increasing areas of asymmetrical cortical involvement in the temporal lobes and frontal lobes. Follow-up MRI 3 years later (G; Axial T2, H; axial and I; coronal T2 FLAIR) showed generalised cerebral atrophy, most marked in the frontal lobes and basal ganglia with exvacuo-dilatation of the lateral ventricles. The high signal is consistent with gliosis. Case 2 MRI (J – M) showed bilateral hyperintensity of striatal nuclei which remained unchanged in subsequent scans. Case 4 brain MRI (N) showed bilateral basal ganglia changes suggestive of a mitochondrial disorder. Extensive skin lesions in Case 4 (O – P).

150x288mm (150 x 150 DPI)

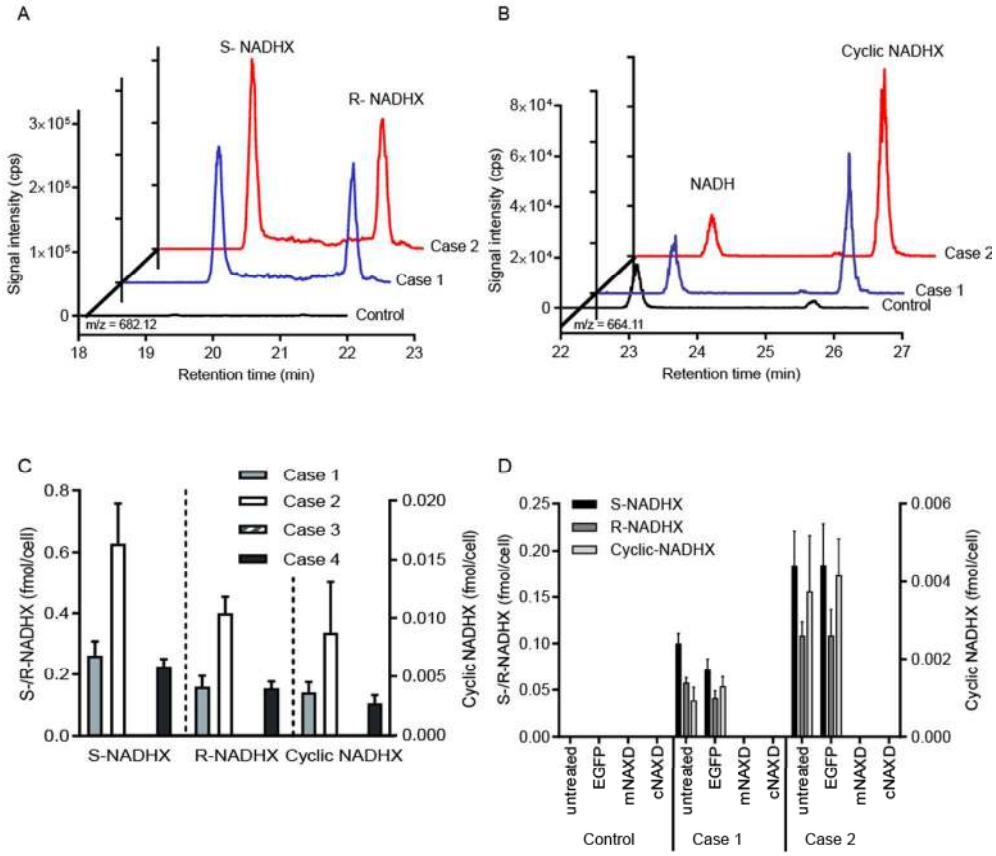

Caption : Fig. 2: NADHX accumulation in subject fibroblasts and phenotypic rescue by lentiviral gene delivery of wild-type NAXD‼ ┼ Representative examples of LC-MS extracted ion chromatograms of A) S- and R-NADHX metabolites (XIC = 682.12) and B) NADH and cyclic NADHX (XIC = 664.11). The chromatograms clearly show peaks of S-, R- and cyclic NADHX in Case 1 and Case 2, and not in a control. C) Quantitative results of the NADHX measurements after cultivation of fibroblasts from Cases 1, 2, 3 and 4 under standard conditions at 37°C for 96 hours. Note that these metabolites were not detected in four control fibroblast lines. Data is mean +/- SD, n = 3. C) Quantitative results of the NADHX measurements in lentiviral-rescued cells. There was a clear accumulation of S-, R- and cyclic NADHX in Case 1 and Case 2, independently of transduction with GFP-only vectors. S-, R- and cyclic NADXH were not detected in control fibroblasts. Lentiviral gene rescue with either the mNAXD or cNAXD construct completely prevented accumulation of S-, R- and cyclic NADHX in subject cells. Data is mean +/- SD, n = 3.‼ ┼

174x154mm (150 x 150 DPI)

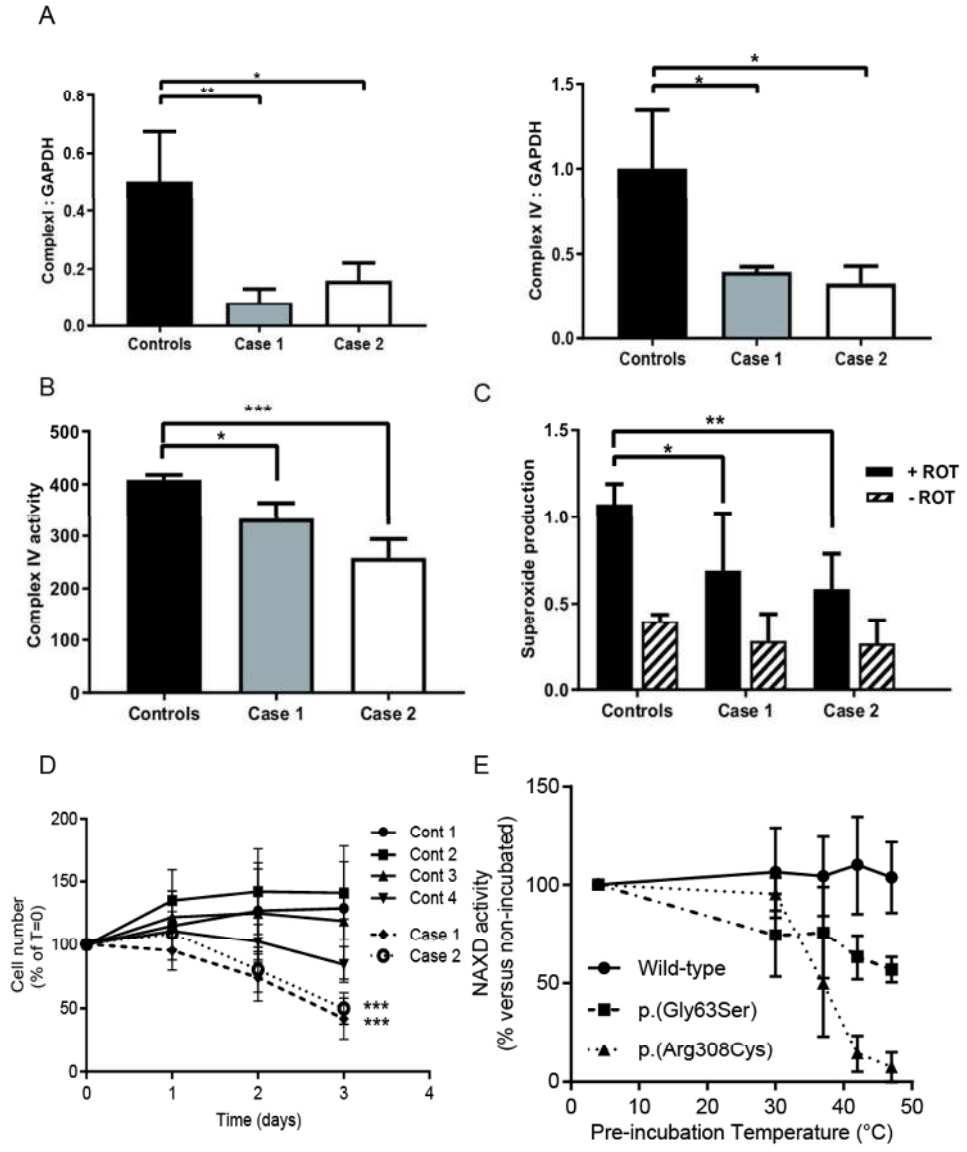

Fig. 3 - Mitochondrial impairment in NAXD subject fibroblasts and thermostability of recombinant NAXD protein variants

A) Mitochondrial OXPHOS proteins were separated by SDS-PAGE, probed for relative expression levels of key OXPHOS subunits by immunoblotting, and expression levels normalized to GAPDH as a loading control. There was a significant decrease in the expression of Complex I and Complex IV proteins expression in Case 1 and Case 2 compared to controls. B) Mitochondrial OXPHOS enzyme activity was measured in cell extracts by immunocapture dipstick assays. There was a significant decrease in Complex IV activity (mAbs/mg protein) in Case 1 and Case 2 relative to controls. C) Relative rates (relative fluorescent units/time) of mitochondrial superoxide production in fibroblasts was measured with the superoxide sensitive probe dihydroethidium in the presence or absence of the Complex I inhibitor rotenone. D) Growth rate in medium devoid of glucose but containing 5mM galactose and 50μM sodium azide was normalized to growth rate in basal medium to account for variation in the baseline growth rate of each cell line. The normalized growth rate in Case 1 and Case 2 was significantly lower than controls. E) Purified recombinant NAXD protein, without or with missense mutations p.(Gly63Ser) and p.(Arg308Cys), was pre-incubated at the indicated temperature for 30 min prior to addition to a reaction mixture for the spectrophotometric assay of NADHX

dehydratase activity. Data is mean ± SD, n>3 per measurement from at least two independent experiments. Statistical significance was determined using one-way ANOVA with Bonferroni correction for multiple comparisons, * P<0.05; **P<0.01; *** P<0.001.

168x196mm (150 x 150 DPI)

Supplementary material

Supplementary Table 1: *In silico* analysis of *NAXD* variants

	Variant	Inheritance	Population frequency GnomAD (mean allele frequency)	*NAXD* variants				Consequence
				chr:position	Coding region	cDNA (NM_001242882.1)	Protein (NP_001229811)	
Case 1	splicing site SNV	AR/ compound het (mat.)	0	chr13:111289597	intron 9	c.839+1G>T	p.(?)	most likely affects splicing
	nonsyn. SNV	AR/ compound het (pat.)	17 het 0 hom (6.919e-5)	chr13:111290807	exon 10	c.922C>T	p.(Arg308Cys)	missense
Case 2	nonsyn. SNV	AR/ compound het (mat.)	0	chr13:111274703	exon 2	c.187G>A	p.(Gly63Ser)	missense
	2-bp insertion	AR/ compound het (pat.)	2 het 0 hom (8.173e-6)	chr13:111290833	exon 10	c.948_949insTT	p.(Ala317Leufs*64)	frameshift and stop loss
Case 3	4-bp deletion	AR/ hom	13 het 0 hom (4.742e-5)	chr13:111274567	exon 2	c.51_54delAGAA	p.(Ala20Phefs*9)	frameshift and probable nonsense-mediated decay
Case 4	nonsyn. SNV	AR/ hom	11 het 0 hom (4.473e-5)	chr13:111277601	exon 4	c.308C>T	p.(Pro103Leu)	missense
Case 5	4-bp deletion	AR/ hom	0	chr13:111274570	exon 2	c.54_57delAAGA	p.(Ala20Phefs*9)	frameshift and premature

								truncation
Case 6	nonsyn. SNV	*De novo*	0	chr13:111277624	exon 4	c.331C>T	p.(Leu111Phe)	missense
	nonsyn. SNV	*De novo*	0	chr13:111289533	exon 9	c.776T>G	p.(Leu259Arg)	missense

All genomic coordinates are in UCSC hg19. AA: amino acid. AR: Autosomal Recessive. Het: heterozygote. Hom: homozygote. Mat: maternally inherited. Nonsyn: nonsynonymous. Pat: paternally inherited.

Supplementary Table 2: *In silico* analysis of NAXD variants

			Genebank transcript ID	NM_001242882.1	NM_001242883.1	NM_001242881.1	NM_018210.3
			Ensembl transcript ID		ENST00000424185		ENST00000309957
			Transcript variant	variant 4	variant 4	variant 2	variant 1
			Size (base pairs)	2599	2313	2602	2738
			Genebank protein ID	NP_001229811	NP_001229812	NP_001229810	NP_060680
			Protein isoform	isoform c	isoform d	isoform b	isoform a
			Protein length (amino acids)	329	237	347	390
			Genomic start (chr 13)	111267807	111267807	111267931	111267931
			Genomic end (chr 13)	111292342	111292342	111292342	111292342
			Relative expression (based on EST)	81%	19%	8%	0%
	Variant	**GnomAD population frequence (MAF)**	**Comments**	This variant (3) differs in the 5' UTR and 5' coding region, uses an alternate start codon, and uses an alternate splice site that causes a frameshift in the 3' coding region, compared to variant 1. The encoded isoform (c) has distinct N- and C-termini and is shorter than isoform a.	This variant (4) differs in the 5' UTR and 5' coding region, uses an alternate start codon, and uses an alternate splice site that causes a frameshift in the 3' coding region, compared to variant 1. The encoded isoform (d) has distinct N- and C-termini and is shorter than isoform a.	This variant (2) uses an alternate splice site that causes a frameshift in the 3' coding region, compared to variant 1. The encoded isoform (b) has a distinct and shorter C-terminus, compared to isoform a.	This variant (1) represents the longest transcript and encodes the longest isoform (a).
Case 1: Compound heterozygous	**splicing site SNV NC_000013.10:g.111 289597 G>T**	0	Coding region	intron 9	intron 6	intron 9	intron 9
			cDNA position	c.839+1G>T	c.563+1G>T	c.893+1G>T	c.893+1G>T
			HSF3	Alteration of the WT donor site	Alteration of the WT donor site	Alteration of the WT donor site	Alteration of the WT donor site
			Consequence	Most likely affects splicing	Most likely affects splicing	Most likely affects splicing	Most likely affects splicing
	missense SNV NC_000013.10:g.111 290807 C>T	17 heterozygotes 0 homozygotes (6.919e-5)	Coding region	exon 10	exon 7	exon 10	exon 10
			cDNA position	c.922C>T	c.646C>T	c.976C>T	c.1112C>T
			AA change	p.(Arg308Cys)	p.(Arg216Cys)	p.(Arg326Cys)	p.(Ser371Leu)
			Provean	n/a	probably deleterious (-7.32)	n/a	probably neutral (-0.18)
			SIFT	n/a	damaging (0.000)	n/a	damaging (0.022)
			PolyPhen2	probably damaging (1.000)	probably damaging (1.000)	probably damaging (1.000)	benign (0.299)
			Consequence	missense	missense	missense	missense
Case 2:Compound heterozygous	**missense SNV NC_000013.10:g.111 274703 G>A**	0	Coding region	exon 2	intron 1	exon 2	exon 2
			cDNA position	c.187G>A	c.57-5083G>A	c.241G>A	c.241G>A
			AA change	p.(Gly63Ser)	n/a	p.(Gly81Ser)	p.(Gly81Ser)
			Provean	n/a	n/a	n/a	probably deleterious (-5.73)
			SIFT	n/a	n/a	n/a	damaging (0.00)
			PolyPhen2	probably damaging (1.000)	n/a	probably damaging (1.000)	probably damaging (1.000)
			Consequence	missense	n/a	missense	missense
	2-bp insertion NC_000013.10:g.111	2 heterozygotes 0 homozygotes	Coding region	exon 10	exon 7	exon 10	exon 10
			cDNA position	c.948_949insTT	c.672_673insTT	c.1002_1003insTT	c.1138_1139insTT

	290833_111290834insTT	(8.173e-6)	AA change	p.(Ala317Leufs*64)	p.(Ile224*)	p.(Ile334*)	p.(Arg380LeufsTer15)
			Consequence	frameshift and c-terminal truncation	frameshift and c-terminal truncation	frameshift and c-terminal truncation	stop codon lost, prolonged protein
Case 3: Homozygous	**NC_000013.10:g.111274567_111274570delAGAA**	13 heterozygote 0 homozygotes	Coding region	Exon 2	Intron 1	Exon 2	Exon 2
			cDNA position	c.51_54delAGAA	c.57-5219_57-5216delAGAA	c.105_108delAGAA	c.105_108delAGAA
			AA change	p.(Ala20Phefs*9)	n/a	p.(Ala38Phefs*9)	p.(Ala38Phefs*9)
			Consequence	Frameshift and probable nonsense-mediated decay	n/a	Frameshift and probable nonsense-mediated decay	Frameshift and probable nonsense-mediated decay
Case 4: Homozygous	**NC_000013.10:g.111277601C>T**	11 het 0 hom (4.473e-5)	Coding region	Exon 4	Intron 1	Exon 4	Exon 4
			cDNA position	c.308C>T	c.57-2185C>T	c.362C>T	c.362C>T
			AA change	p.(Pro103Leu)	n/a	p.(Pro121Leu)	p.(Pro121Leu)
			Provean	Deleterious (-9.10)	n/a	Deleterious (-9.25)	Deleterious (-9.25)
			SIFT	Damaging (0.00)	n/a	Damaging (0.00)	Damaging (0.00)
			PolyPhen2	Probably damaging	n/a	Probably damaging	Probably damaging
			Consequence	Missense	n/a	Missense	Missense
Case 5: Homozygous	**4-bp deletion NC_000013.10:g.111274570_111274573delAAGA**	0	Coding region	exon 2	intron 1	exon 2	exon 2
			cDNA position	c.54_57delAAGA	c.57-5216_57-5213delAAGA	c.108_111delAAGA	c.108_111delAAGA
			AA change	p.(Ala20Phefs*9)	n/a	p.(Ala38Phefs*9)	p.(Ala38Phefs*9)
			Consequence	frameshift and premature truncation	n/a	frameshift and premature truncation	frameshift and premature truncation
Case 6: *De novo*	**De novo missense NC_000013.10:g.111277624 C>T**	0	Coding region	Exon 4	Intron 1	Exon 4	Exon 4
			cDNA position	c.331C>T	c.57-2162C>T	c.385C>T	c.385C>T
			AA change	p.(Leu111Phe)	n/a	p.(Leu129Phe)	p.(Leu129Phe)
			Provean	Deleterious	n/a	Deleterious	Deleterious (-3.78)
			SIFT	Damaging	n/a	Damaging	Damaging (0.028)
			PolyPhen2	possibly damaging(0.519)	n/a	possibly damaging(0.519)	possibly damaging(0.519)
			Consequence	missense	n/a	missense	missense
	De novo missense NC_000013.10:g.111289533 T>G	0	Coding region	Exon 9	Exon 6	Exon 9	Exon 9
			cDNA position	c.776T>G	c.500T>G	830T>G	c.830T>G
			AA change	p.(Leu259Arg)	p.(Leu167Arg)	p.(Leu277Arg)	p.(Leu277Arg)
			Provean	Deleterious (-5.62)	Deleterious (-5.73)	n/a	Deleterious (-5.70)
			SIFT	Damaging (0.00)	Damaging (0.00)	n/a	Damaging (0.00)
			PolyPhen2	probably damaging (1.00)	probably damaging (1.00)	probably damaging (1.00)	probably damaging (1.00)
			Consequence	missense	missense	missense	missense

Supplementary Table 3: Kinetic properties of *NAXD* missense variants

	WT		p.(Gly63Ser)		p.(Arg308Cys)	
	Vmax (µmol/min/ mg protein)	Km (µM)	Vmax (µmol/min/ mg protein)	Km (µM)	Vmax (µmol/min/ mg protein)	Km (µM)
Average	0.877	8.62	0.261***	28.3**	0.350***	18.8
SD	0.124	1.50	0.017	6.9	0.098	6.2

Data are means ± SD, n ≥ 3 per measurement from at least three independent experiments. NADHX dehydratase activity was assayed spectrophotometrically by monitoring the consumption of S-NADHX. Statistical significance was determined using one-way ANOVA with Bonferroni correction for multiple comparisons, significance is vs wild-type, **P<0.01; *** P<0.001.

Supplementary Table 4: Primer sequences

Primer pair	Primer pair used for	Forward primer (5' to 3')	Reverse primer (5' to 3')
Case 1: splicing variant	gDNA confirmation of NC_000013.10:g.111289597 G>T	CTGCGTGTCTTGGTTTCC	AGAGGGTTCGTCTGTGCC
Case 1: missense variant	gDNA confirmation of NC_000013.10:g.111290807 C>T	AGGGCTAAGCAGCTTGTG	GTGCCTGTTTACTTCTGGTCT
Case 2: missense variant	gDNA confirmation of NC_000013.10:g.111274703 G>A	TGTAAAACGACGGCCAGTAGAGGGTTTTGGTTAATGGGCT	AGCGTGAATGACAGTCAGGT
Case 2: 2bp insertion	gDNA confirmation of NC_000013.10:g.111290833_111290834insTT	TGTAAAACGACGGCCAGTCTGCTTTCTCCTCAGGGGC	GGGTCCGGATTTTCCCATCA
Case 3: 4bp deletion	gDNA confirmation of NC_000013.10:g.111274567_111274570delAGAA	AGAGGGTTTTGGTTAATGGG	CAGCTACTTACTCCTGACAG
Case 4: missense variant	gDNA confirmation of NC_000013.10:g.111277601C>T	CAGTGGCGGCAAAAGTCTTTC	CGCCGTCTCTGTCTTATTCTGA
Case 5: 4bp deletion	gDNA confirmation of NC_000013.10:g.111274570_111274573delAAGA	TGTAAAACGACGGCCAGTAGAGGGTTTTGGTTAATGGGCT	AGCGTGAATGACAGTCAGGT
Case 6: missense variant #1	gDNA confirmation of NC_000013.10:g.111277624 C>T	CCTGTGCAGTGCTTGTGTG	TTTCTGTGGTCCAGCAAGG
Case 6: missense variant #2	gDNA confirmation of NC_000013.10:g.111289533 T>G	TCACATTCACACACATGGC	GCTACTTATTCAACGCATGAGCTAC
Case 1 RT-PCR analysis	RT-PCR for splicing analysis of g.13:111289597 G > T	AGACTGTATGACGCTGTGCTC	GAAGGCTTGGTGGTTGCACT
Case 1 missense variant	Site-directed mutagenesis	CTTCCAGAAGCACGGTTGCTCCACCACCTCCG	CGGAGGTGGTGGTGGAGCAACCGTGCTTCTGGAAG
Case 2 missense variant	Site-directed mutagenesis	GAATAGGCGTAGTTGGAAGCTGTCAGGAGTACACTG	CAGTGTACTCCTGACAGCTTCCAACTACGCCTATTC

NAXD-mito	Amplification of NAXD cDNA (mitochondrial isoform) for creation of Gateway Entry clone	GGGGACAAGTTTGTACAAAAAAGCAGGCTTCATGGCCCTGGGTCCTCGCTG	GGGGACCACTTTGTACAAGAAAGCTGGGTCTCAGGTTTCAAAGAGCTTGCTGAAGG
NAXD-cyto	Amplification of NAXD cDNA (cytosolic isoform) for creation of Gateway Entry clone	GGGGACAAGTTTGTACAAAAAAGCAGGCTTCATGGAAAATACTTTGCAGCTGGTGAG	GGGGACCACTTTGTACAAGAAAGCTGGGTCTCAGGTTTCAAAGAGCTTGCTGAAGG
NAXD-pcDNA3.1	DNA sequence confirmation	TAATACGACTCACTATAGGG	TAGAAGGCACAGTCGAGG
pDONR221-NAXD	DNA sequence confirmation of Gateway Entry clones	TGTAAAACGACGGCCAGT	CAGGAAACAGCTATGACC
pDEST-NAXD	DNA sequence confirmation of Gateway bacterial expression constructs	TAATACGACTCACTATAGGG	CTGGCTTGCACGTGTATA

Supplementary Table 5: Scan range, extracted ions and retention time.

ID	Mass [m/z]	Scan range	Formula [M]	Start [min]	End [min]
NAD	662.10184	661.6 – 662.6	C21H27N7O14P2	19.50	23.00
NADH/cyc NADHX	664.11749	663.6 – 664.6	C21H29N7O14P2	22.50	40.00
NADHX	682.12806	681.6 – 682.6	C21H31N7O15P2	19.00	24.50
NADP	742.06817	741.5 – 742.5	C21H28N7O17P3	2.00	5.00
NADPH/cyc NADPHX	371.53827	371.0 – 372.0	C21H30N7O17P3	16.50	24.00
NADPHX	380.54356	380.0 – 381.0	C21H32N7O18P3	0	14.00

Supplementary Table 6: Isotopomer distribution in patient samples and standards.

A comparison of the isotopomer distribution found in patient samples and standards, and calculated based on the molecular formula of the target metabolites (Patiny and Borel, 2013).

Most abundant massed (Da/eV)	Patient pooled sample	Chemically pure standard	Mass prediction
S/R-NADHX			
	682.12683	682.12683	682.12751
	683.13062	683.13062	683.13087
	684.13220	684.13196	684.13176
Cyc NADHX			
	664.11658	664.11652	664.11655
	665.12012	665.12000	665.12030
SD	666.12366	666.12183	666.12365

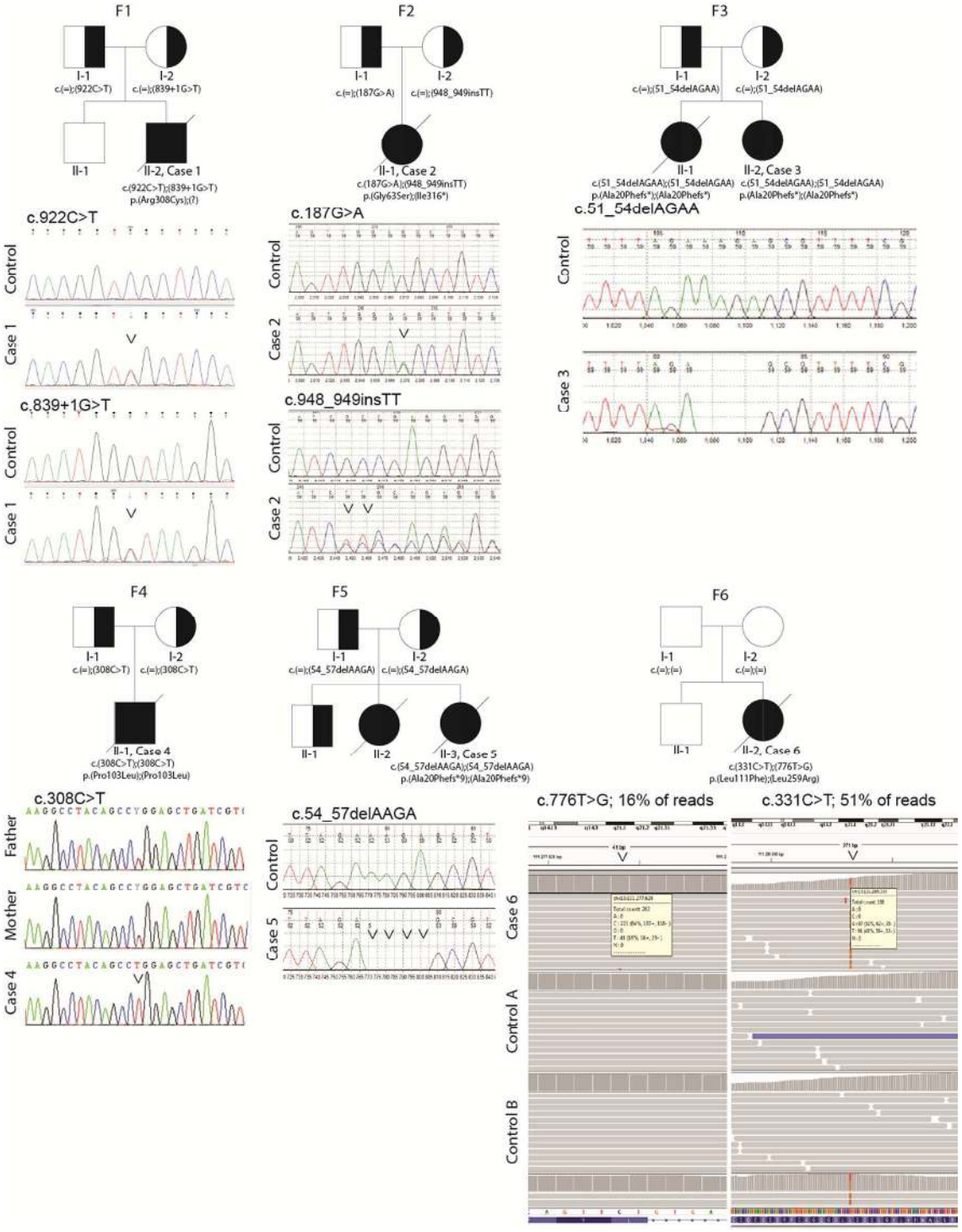

Supplementary Fig. 1- Sanger confirmation and sequence analysis

Sanger confirmation sequencing for Cases 1, 2, 3, 4 and 5, and IGV screenshots for variants in Case 6.

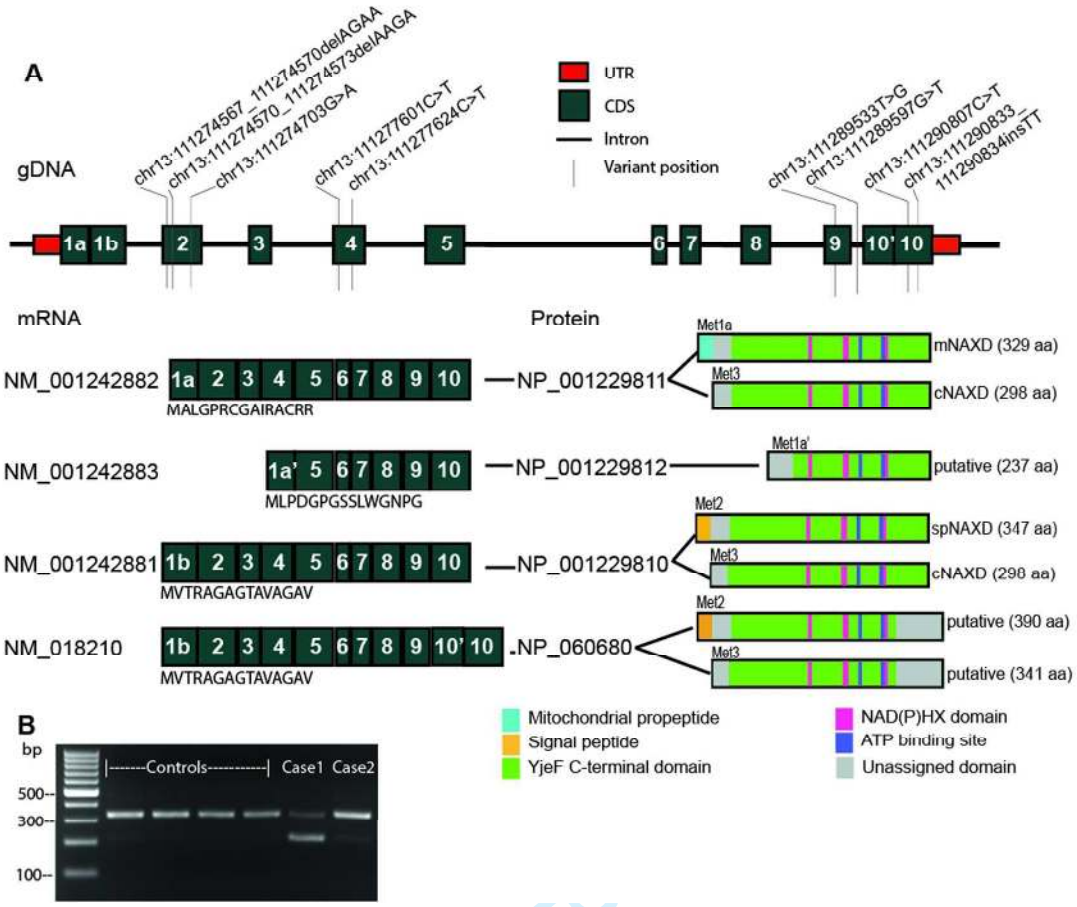

Supplemental Fig.2 – Genetic findings in six NAXD-deficient families

A) Genomic organization of *NAXD* with known subject variants indicated. Predicted transcripts and resulting proteins with predicted protein domains are indicated. The different predicted transcription/translation start sites are also shown (Met1-3). Predicted protein domains (from Uniprot Q8IW45) include; mitochondrial propeptide in blue, signal peptide in orange, YjeF c-terminal domain in green, NAD(P)HX domain in pink, ATP binding site in purple and unassigned domain in grey. mNAXD, mitochondrially targeted NAXD isoform; cNAXD, cytosolic NAXD isoform; spNAXD, ER targeted NAXD isoform. Supplementary Fig. 3 contains a full protein alignment including subject variant analysis. B) Reverse transcription-PCR analysis demonstrated a splicing defect in Case 1 that was not present in Case 2 or four controls. Confirmatory Sanger for RT-PCR fragments can be found in Supplementary Fig. 4.

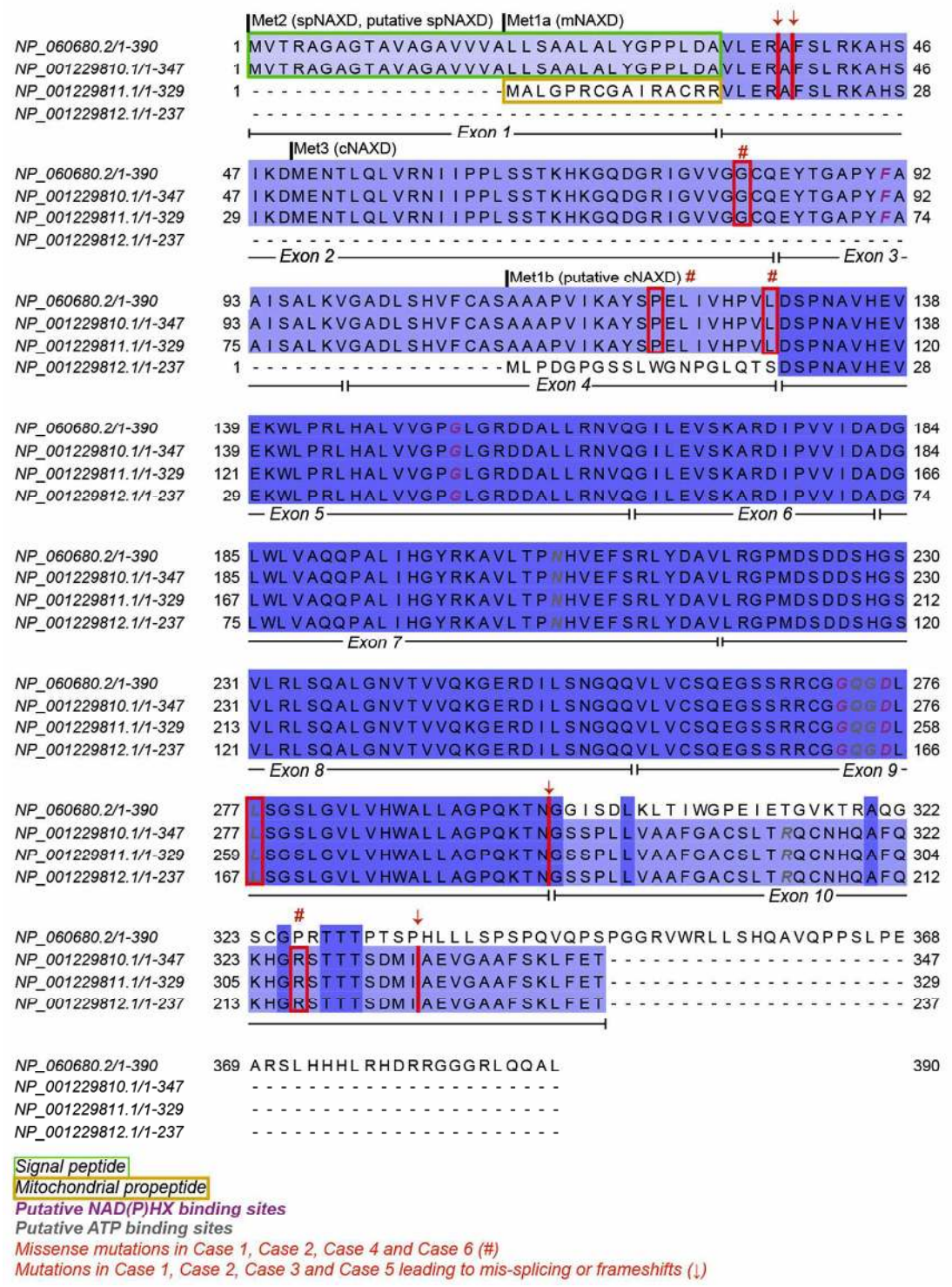

Supplementary Fig. 3 – Protein sequence alignment of predicted human NAXD isoforms

Start sites (Met1-3) are indicated for the different isoforms using the nomenclature described in the supplementary text. The exon structure corresponding to the spNAXD and mNAXD

isoforms is also shown. Isoforms are indicated as 'putative' in case of weak support from EST data. This is the case for the shortest predicted isoform (NP_001229812; 237 aa; putative cNAXD) and even more for the longest predicted isoform (NP_060680; 390 aa; putative spNAXD). Accordingly, several subject mutations identified in this study occur in sequence locations that are not conserved in the putative cNAXD or putative spNAXD isoforms. c, cytosolic; m, mitochondrial; sp, signal peptide.

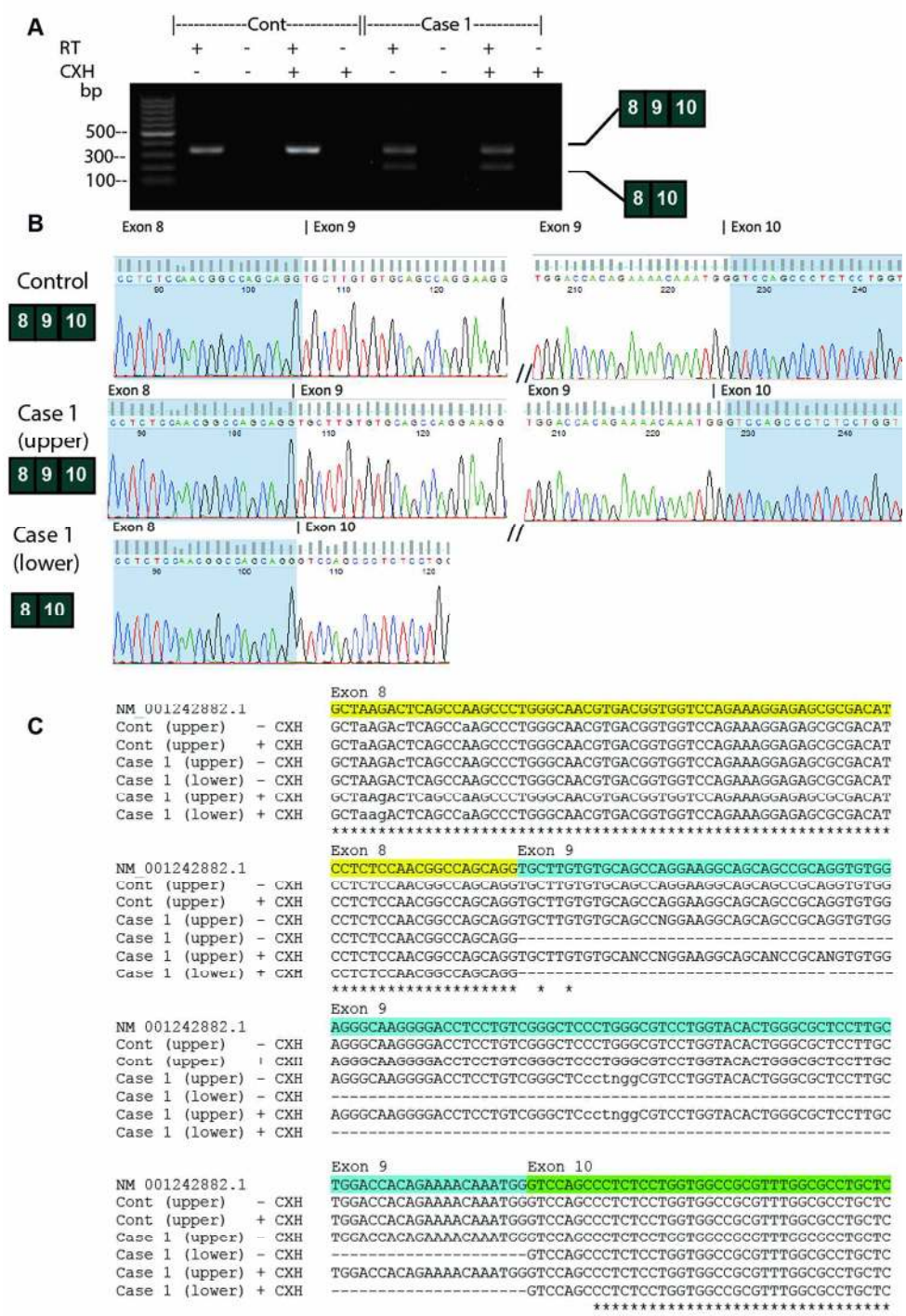

Supplementary Fig. 4- Splice analysis for Case 1

RT-PCR analysis for Case 1 (c.839+1G>T) splice site variant. A) RT-PCR analysis identified an additional band in Case 1 that was not present in controls. B) Sanger sequencing and C)

sequence alignment confirmed skipping of Exon 9. CXH; cycloheximide, RT; reverse-transcription.

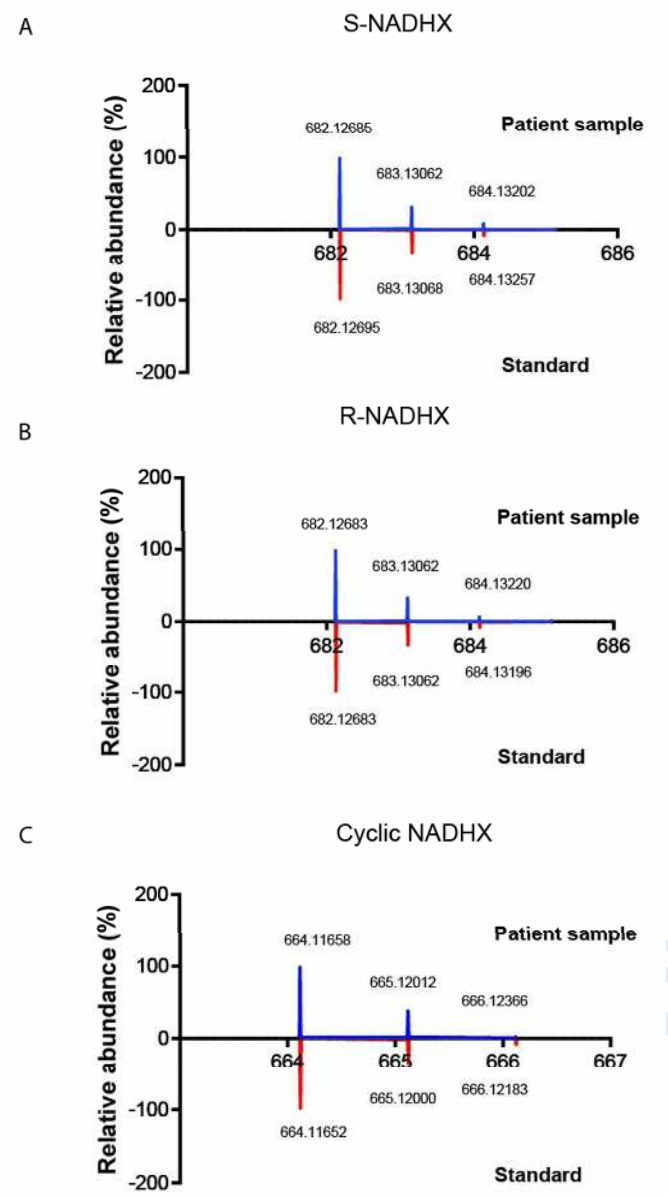

Supplementary Fig. 5 – NADHX identification in patient fibroblast extracts

Isotope distribution of A) S-NADHX, B) R-NADHX and C) cyclic NADHX found in pooled subject samples (case 1 and case 2, above) compared to the pattern in a chemically pure standard, below. The numbers shown correspond to the measured accurate masses. Spectra were taken at retention time of 19.37 (S-NADHX), 21.33 (R-NADHX), and 26.85 (cyclic NADHX) min, respectively, at a resolution of 140 000. A comparison of the isotopomer distribution found in patient samples and standards, and calculated based on the molecular formula of the target metabolites is given in Supplementary Table 5 and 6.

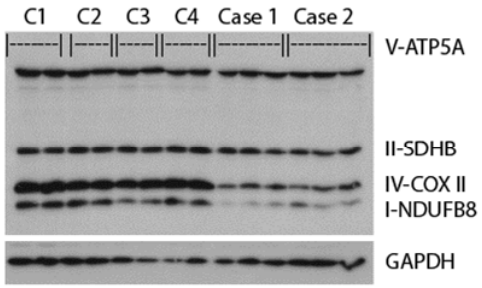

Supplementary Fig. 6 – OXPHOS protein subunit expression in Case 1 and Case 2 fibroblasts.

A representative western blot used for analysis of mitochondrial OXPHOS subunit expression in fibroblasts from four paediatric control subjects compared to Case 1 and Case 2. Quantification results are presented in Fig. 3A.

Materials and Methods

Subjects

All procedures followed were in accordance with the ethical standards and approved by human research ethics committees (institutional and national) and with the Helsinki Declaration of 1975, as revised in 2000. Written informed consent was obtained from all participants or their legal guardians of all individuals investigated in this study.

Subjects were recruited independently from each institute. Case 1 was recruited as part of a gene discovery program in children with undiagnosed neurological disease. Whole exome sequencing was used to identify candidate genes. Potential genes were submitted to Matchmaker Exchange, an international database to match subjects of similar phenotype and potential pathogenic variants (Philippakis *et al.*, 2015). Through Matchmaker Exchange a further two subjects were identified with potential pathogenic variants in *NAXD*. Three additional cases were identified through collaborations.

Variant annotation and filtering for Case 1

Genomic DNA from whole blood cells was collected in the subjects and their family members using the QIAamp DNA mini kit (Qiagen, Hilden, Germany), following the manufacturer's instructions.

For Case 1, the proband was sequenced using Whole Exome Sequencing (WES) and primary bioinformatics processed including short sequence read alignment and variant calling on all sequenced samples. Variants were annotated with Annovar (Wang *et al.*, 2010) and filtered based on frequencies from ExAC (Lek *et al.*, 2016), GnomAD (Lek *et al.*, 2016), 1,000 Genomes Project (Genomes Project *et al.*, 2015) and internal WES datasets at the Children's Hospital of Philadelphia. Variants were selected based on the following criteria; amino acid changing (non-synonymous/stop-gain SNVs, indels, and splicing site variants within 10-bp of exon-intron boundaries), ExAC allele frequency below 1×10^{-5}, predicted to be deleterious in SIFT, damaging in PolyPhen2, and conserved in PhyloP, and with balanced alleles for heterozygous calls (depth ratio below 3:1). *In silico* analysis by SIFT (Kumar *et al.*, 2009) and PolyPhen-2 (Adzhubei *et al.*, 2010) determined the likely pathogenicity of variants. The evolutionary conservation of genomic regions around the variants was analysed using PhyloP (Cooper *et al.*, 2005). For single sample analysis, homozygous as well as compound heterozygous variants, both indicative of a recessive inheritance, were discarded if the alternative allele's population frequency in either of the ExAC, 1000 Genomes or internal

datasets was greater than 0.5%; and heterozygous variants, in this case dominant de novo candidates, were discarded if the alternative allele frequency was greater than 0.1%. Confirmatory Sanger sequencing was completed in genomic DNA samples from all available family members using the primers listed in Supplementary Table 1.

Variant annotation and filtering for Case 2 and Case 5

We undertook trio WES of the affected child and unaffected, unrelated parents. Genomic DNA samples were quantified according to manufacturer's instructions on the Qubit fluorimeter (Thermo Fisher Scientific, Massachusetts, USA) to determine that the minimum quantity of DNA required, 3000ng, was available. The samples were fragmented using the Bioruptor (Diagenode, Liège, Belgium), and indexed adaptors ligated before hybridization with the Agilent SureSelect All Exon capture kit (v4, v5 or v6) or Agilent SureSelect Focused exome kit (Santa Clara, CA, USA). Paired-end 100-bp reads were sequenced on a HiSeq 2500 (Illumina, San Diego, CA, USA). The Illumina HiSeq fastq sequencing reads were de-multiplexed and aligned to the reference (GRCh37/Hg19) using BWA-MEM (v0.7.12), converted to BAM format file, and subjected to duplicate removal using Picard (v1.129). GATK (v3.4-46) was used for indel re-alignment, variant calling and quality filtering. Variants were annotated using Alamut-Batch (v1.4.4), a Variant Call Format (VCF) file was submitted and all SNVs and indels were annotated using a range of different variant and genomic databases, including HGMD Professional (Stenson *et al.*, 2009). An in-house bioinformatics pipeline was used to identify *de novo*, compound heterozygous or homozygous rare variants with a MAF <0.0001 (<0.01%) in ExAC or the Exome variant server (EVS http://evs.gs.washington.edu/EVS/). Variants were restricted to non-synonymous variants, those affecting the conserved splice sites or those within−50/+10 base pairs of flanking exons predicted by Alamut-Batch to affect splicing (five tools were used: SpliceSiteFinder-like, MaxEntScan, NNSplice (Fruitfly), GeneSplicer and Human Splicing Finder). Variants annotated as pathogenic in HGMD Pro were retained regardless of other filtering criteria. Copy number variants were identified using read depth analysis with a modified version of R software package ExomeDepth (v1.1.8) (Plagnol *et al.*, 2012) and comparing the test sample against reference samples.

Variant annotation and filtering for Case 3

For Case 3 WES was performed from the DNA of proband and parents with Illumina's Nextera Rapid Capture Exome Kit and the samples were processed on the Illumina NextSeq Platform (Illumina, San Diego, California, USA). The average coverage depth was 130x, with ~95% of the bases covered at >20x, and a sensitivity of >90% (Girisha *et al.*, 2016). Data were stored and analyzed using a previously-published automated pipeline, SeqMule v1.2.5 (Guo *et al.*, 2015). The variant call format (.vcf) file was annotated by ANNOVAR v.2016Feb01 (Danecek *et al.*, 2011). Variants were filtered to 1% minor allele frequency in population databases including ExAC, 1,000 genome database, and an internal WES database of 405 individuals of Indian origin. Exonic and splice site variants were then prioritized by OMIM (Online Mendelian Inheritance in Man) identity, phenotypic assessment, and the American College of Medical Genetics (ACMG) criteria of pathogenicity (Richards *et al.*, 2015). Validation was done using Sanger sequencing for proband and the parents for the candidate variant.

Variant annotation and filtering for Case 4

WES was performed as follows; coding regions were enriched with Nextera Rapid Exome Capture (Illumina) and sequenced with 100 bp paired-end reads on an Illumina NextSeq500 sequencer and aligned to the human reference genome (UCSC hg38). Variants were restricted to a minor allele frequency of less than or equal to 0.01 (1%) from in-house controls and external variant databases included ExAC, EVS and 1,000 Genomes Project. Autosomal recessive (homozygous or compound heterozygous) variants in nuclear genes encoding mitochondrial-targeted proteins were prioritised. PolyPhen-2, SIFT and CADD were used to assess the pathogenicity of candidate variants.

Variant annotation and filtering for Case 6

Genomic DNA was isolated from whole blood cells of the subject and her parents using the chemagic DNA Blood Kit special (PerkinElmer, Waltham, USA) according to the manufacturer's protocol. Exonic regions were enriched using the SureSelect Human All Exon kit (AG_60Mb_v6) from Agilent followed by sequencing as 100 bp paired-end runs on an Illumina HiSeq2500. Reads were aligned to the human reference genome (UCSC Genome Browser build hg19) using Burrows-Wheeler Aligner (v.0.7.5a). Detection of single-nucleotide variants and small insertions and deletions (indels) was performed with SAMtools (version 0.1.19). For analysis of rare bi-allelic variants, only variants with a minor allele

frequency (MAF) of less than 1% in the Munich in-house database consisting of 14,000 exomes were considered. For investigations on *de novo* variants, filtering for variants which were present solely in the subject but not in the parents was performed.

NAXD gene, transcript analysis and predicted protein structure

The human *NAXD* gene contains 10 exons, is located on chromosome 13 and is predicted to generate four coding transcripts and two non-coding transcripts (Fig. 2B). The gene has two alternative splice sites at the 3' end of exon 1, resulting in transcripts containing either the first half (Fig. 2B; exon 1a in NM_001242882 and exon 1a' in NM_001242883) or the second half of this exon (exon 1b in Fig. 2B; NM_001242881 and NM_018210). One transcript does not retain exons 2 – 4 (NM_001242883) and one transcript includes a 5' extension on exon 10 (exon 10' in Fig. 2B; NM_018210). Exon 1 has three putative ATG start codons: Met1a in exon 1a (used in NM_001242882), Met1a' in exon1a' (used in NM_001242883), and Met2 in exon 1b (used in NM_001242881 and NM_018210). The second exon also contains a highly conserved ATG codon, Met3 (Marbaix *et al.*, 2014), which is present in three of the four transcripts (except NM_001242883). Transcription initiation at these different sites and differential splicing are thus predicted to lead to expression of the four mRNA transcripts encoding a 329 aa protein with a predicted mitochondrial propeptide (mNAXD; NM_001242882; NP_001229811), a 347 aa protein identical to mNAXD except for the N-terminus predicted to correspond to a signal peptide (spNAXD; NM_001242881; NP_001229810), a putative NAXD 237 aa protein (NM_001242883; NP_001229812), with a shorter and different N-terminus than mNAXD and spNAXD, and a putative NAXD 390 aa protein (NM_018210; NP_060680) identical to spNAXD in N-terminus, but with a different and extended C-terminus (Fig. 2B and Supplementary Fig. 1). Finally, leaky mRNA scanning of the three longest transcripts is expected, in addition to synthesis of the mitochondrial or endoplasmic reticulum-targeted proteins, to lead to formation of a shorter cytosolic form (cNAXD; 298 aa protein from mNAXD and spNAXD mRNAs) when translation is initiated from the downstream Met3 codon instead of Met1a or Met2 (Fig. 2B and Supplementary Fig. 1), as previously suggested (Marbaix *et al.*, 2014). Western blotting using two different commercial human NAXD antibodies and a mouse Carkd antibody against a conserved region failed to detect specific endogenous protein in subject fibroblast extracts, similarly to what was previously reported for the mouse homologue Carkd using tissue extracts(Marbaix *et al.*, 2014). This technique

could therefore not be used to explore which of the predicted isoforms is actually expressed in human fibroblasts. Expressed sequence tag (EST) analysis (UCSC Genome Browser on the Human (GRCh38/hg38) Assembly accessed on February 12, 2018) predicted the most abundant transcript to correspond to mNAXD (NM_001242882.1) with ~ 81% of the 448 total ESTs considered (Supplementary Table 1). This mNAXD transcript encodes a long (329 aa) mitochondrial protein form (translation start at Met1a) and a shorter (298 aa) cytosolic protein (translation start at Met3), as described above; the mitochondrial protein form shares 82% identity with the mouse Carkd isoform 2 (NP_001177286.1) containing also a mitochondrial propeptide and previously characterized in more detail (Marbaix *et al.*, 2011; Marbaix *et al.*, 2014). Both the short (237 aa) cytosolic isoform (NM_001242883) and the (347 aa) spNAXD isoform (NM_001242881) were represented each by ~ 8% of all transcripts. No clear evidence was found within the EST database in support of the transcript variant carrying both a signal peptide sequence and a 5' extension of exon 10 (NM_018210 encoding the putative 390 aa protein).

NAXD transcript isoform analysis

Four coding and two non-coding transcript variants are predicted for the *NAXD* gene (NCBI Reference Sequences). Alternative splicing and the use of different ATG start codons within the first exon is predicted to lead to the expression of one transcript with an N-terminal mitochondrial targeting signal (NM_001242882), one transcript without an N-terminal targeting sequence (NM_001242883), and two transcripts with an N-terminal signal peptide (NM_001242881 and NM_018210). NM_018210 additionally carries a 5' extension of the last exon (exon 10), leading to a different and longer C terminus. To estimate the relative abundance of the different transcript variants, the more than 600 expressed sequence tags (ESTs) for the *NAXD* gene contained in the UCSC Genome Browser (Human Dec. 2013 (GRCh38/hg38) Assembly; database accessed for analysis on February 12, 2018) were compared to the predicted coding RefSeq transcripts. ESTs are single-read sequences of reverse transcribed RNA that were cloned into plasmids and sequenced. Incomplete reverse transcription and limitation in the read length impedes exact determination of transcript abundance. Therefore, only ESTs spanning *NAXD* exons 1 to 5 were taken into account for our analysis here (including the ones missing exons 2-4, potentially corresponding to transcript NM_001242883). Out of these ~ 450 ESTs, 365, 34, and 38 could be annotated to the NM_001242882, NM_001242881, and NM_001242883 transcripts, respectively.

Interestingly, no EST containing both a signal peptide and the 5' extension of exon 10 were found within this subdataset. Additionally, the number of ESTs containing the 5' extension of exon 10 within the complete dataset (independent of the length of the ESTs) was very limited (7 out of > 600), suggesting that this transcript variant is only expressed at very low levels in humans, if at all.

Cell Culture

Primary cultures of fibroblasts were established from skin biopsies and were cultured in basal medium (high-glucose DMEM (Gibco) with 10% fetal bovine serum (Gibco), 100 units/mL penicillin, and 100 µg/mL streptomycin) at 37°C with 5% CO_2.

RT-PCR analysis

Fibroblasts were cultured in the presence or absence of cycloheximide (100 ng/µL) for 24 hours to prevent nonsense mediated decay in basal media prior to harvesting RNA using a commercially available kit (Qiagen RNeasy kit). cDNA was synthesized using Invitrogen Superscript III first strand mastermix and random hexamers from 200ng RNA per sample. Reverse-transcription PCR (RT-PCR) reactions were performed using custom primers (Supplementary Table 1) and PCR products were extracted from agarose gels followed by Sanger sequencing.

LC-MS analysis of NAD(H), NADP(H), and damaged derivatives

Fibroblasts were seeded in basal media at a density of 5.0 x 10^5 cells in 150 mm dishes or for lentiviral-rescued cells, at 2 x 10^5 cells (untransfected) or 4 x 10^5 cells (transfected) in a 92 mm dish and cultivated for 96 hours, by which time cells were approximately 90% confluent. Parallel dishes were cultured and cells harvested with trypsin and used for cell concentration determination by adding an equal volume of trypan blue in an automated cell counter (Countess, Thermofisher). To extract intracellular metabolites, culture media were aspirated and cells washed once with warm saline solution (0.9% NaCl), then immediately placed on a cooling plate at -20°C. Appropriate volumes (0.5 – 1mL) of ice-cold extraction solution (1:1 methanol:TE (10 mM Tris, 1 mM EDTA, pH 7.0)) were added, cells were collected via scraping and transferred to a 2 ml tube at -20°C. An equal volume of ice-cold chloroform was added and the mixture incubated with shaking at -20°C for 30 minutes, then centrifuged at 10,000 x g and -9°C for 10 minutes. The upper polar phase was filtered through a 0.22 µm

regenerated cellulose membrane (Phoenix). A defined volume of 700 µl was frozen at -80°C prior to lyophilisation (Labconco) at -105°C for 3 hours.

Lyophylised samples were dissolved in 60 µl of 10mM Tris-HCl buffer, pH 8.0. Intracellular metabolite concentrations were measured with an HRAM-RP-LC-MS (high resolution accurate mass reversed phase liquid chromatography mass spectrometry) method using a Dionex UltiMate 3000 (Thermo Fisher Scientific, Waltham, MA, USA) LC coupled to a Qexactive Orbitrap mass spectrometer (Thermo Fisher Scientific, Waltham, MA, USA) equipped with a heated electrospray ionization source. Nitrogen was supplied by an NMG33 generator (CMC). Absolute concentrations were calculated based on external calibration curves prepared in 10 mM Tris-HCl buffer, pH 8.0. Analyte separation was achieved by reversed phase chromatography using a Polaris C18-A column (3 µm, 180 Å, 3.0 X 150 mm; Agilent) equipped with a SecurityGuard™ ULTRA C18 precolumn (for 3.0 mm ID columns; Phenomenex) at a temperature of 20°C. Target metabolites (NAD, NADH, NADP, NADPH, S-NADHX, R-NADHX, cyclic NADHX, S-NADPHX, R-NADPHX, cyclic NADPHX) were eluted at a constant flow rate of 0.2 ml/min in gradient mode, where solvent A was 50 mM ammonium acetate at pH 7 (adjusted by acetic acid addition) and solvent B was acetonitrile, according to the following profile: 0 – 5 min, 0 % B; 5 – 22 min, 0 - 5 % B; 22 – 27 min, 5 - 100 % B; 27 – 28 min, 100 - 0 % B; 28 – 40 min, 0 % B. Dependent on the available cell number in each experiment, either 20 or 40 µl of samples and standards were injected and the autosampler was kept cooled at 10 °C. Mass spectral data were obtained using a scheduled single ion monitoring method in negative mode, at a resolution of 70 000, and AGC target size of 10^5, and a maximum injection time of 500 ms. Target metabolites were identified by accurate mass as well as comparison of retention time and natural isotope distribution against chemically pure standards. Details on scan range, extracted ions and retention time are given in Supplementary Table 3.

Likely due to a sensitivity limitation of the methodology used, NADPHX derivatives could not be detected in any of the cell extracts tested.

NAXD variant cloning

The human full-length *NAXD* cDNA clone was obtained from GenScript (pcDNA3.1 containing the NM_001242882.1 sequence; GenScript Clone ID OHu08429). The two missense mutations (Case 1, NM_ 001242882.1, c.922C>T, p.(Arg308Cys) and Case 2, NM_ 001242882.1, c.187G>A, p.(Gly63Ser)) were introduced using the QuikChange Lightning

Site-Directed Mutagenesis Kit (Agilent) according to the manufacturer's instructions. Wild-type and mutated sequences including the mitochondrial targeting sequence (mNAXD starting at Met1a) or not (cNAXD starting at Met3) were then amplified from the corresponding NAXD-pcDNA3.1 plasmid using primers containing attB1 and attB2 sites. The PCR products were inserted into the Gateway pDONR221 vector (Thermo Fischer Scientific) through a BP clonase reaction (Thermo Fisher Scientific) to generate the desired Entry clones. Bacterial expression plasmids containing either wild-type or mutated *cNAXD* cDNA were obtained by an LR clonase reaction (Thermo Fisher Scientific) between the empty pDest-527 plasmid (pDest527 was a gift from Dominic Esposito; Addgene plasmid # 11518) and the appropriate Entry clones according to the manufacturer's instructions. DNA sequences of all intermediate and final steps were verified by Sanger sequencing. All primers used for cloning and sequence verification are listed in Supplementary Table 2.

Bacterial expression and purification of wild-type and mutant NAXD proteins

Wild-type and mutant forms of the cytosolic NAXD isoform (cNAXD) were then produced, using a bacterial overexpression system, as N-terminally His-tagged proteins, and purified and assayed on the day of extraction from the bacterial cells to prevent enzyme degradation. The S-NADHX substrate was synthesized and purified as previously described (Becker-Kettern *et al.*, 2018) and NAXD enzyme kinetic properties determined using a spectrophotometric assay (Marbaix *et al.*, 2011). Given the instability of the mutant proteins, extraction, purification and enzymatic assay of the recombinant proteins were done on the same day to obtain reproducible results.

Gateway expression plasmids were transformed into One Shot® BL21 Star™ (DE3) Chemically Competent *E. coli* cells (Thermo Fisher Scientific) for production of N-terminally His-tagged NAXD (wild-type or missense variants; cytosolic isoform). Overnight pre-cultures (in LB medium containing 100 µg/ml ampicillin) inoculated from single clones were diluted 50-fold in 500 ml main cultures in the same medium and grown to an optical density of 1.6-3.7 at 37 °C with continuous shaking. Cultures were then put on ice for 30 min and protein expression induced by addition of IPTG at a final concentration of 0.1 mM. Induced cultures were left for 24 hours at 18 °C with shaking and cells were harvested by a 15-min centrifugation at 4500 x g and 4 °C. The cell pellets were resuspended in a lysis buffer containing 25 mM Tris-HCl, pH 8.0, 25 mM NaCl, 0.5 mM PMSF, 1 mM DTT, and 1 x EDTA-free Complete Ultra protease inhibitor cocktail (Roche). Cells were either lysed by

sonication (0.5-sec pulses separated by 2.5-sec breaks for 2 min; 25—30% amplitude) or by three freeze/thaw cycles in the presence of 1 mg/ml lysozyme (Sigma Aldrich) followed by a 40-min DNase treatment on ice (100 µg/ml DNase I, 10 mM $MgSO_4$). Lysates were centrifuged for 35 min at 17,000 x g and 4 °C and supernatants filtered on cellulose acetate membranes (0.45 µm pore size; Minisart).

The filtered protein extracts were loaded onto nickel-containing Protino Ni-TED 150 gravity flow columns (Machery-Nagel) and purified according to the manufacturer's instructions. Elution fractions of interest were desalted on Zeba spin columns (7K MWCO, 0.5 ml, Thermo Fisher Scientific) according to the supplier's protocol using a buffer containing 25 mM Tris, pH 7.4 and 25 mM NaCl. All the above purification steps were performed at 4°C. Protein purity and identity was assessed by SDS-PAGE and Western blotting, and protein concentration was determined using a standard Bradford assay (Biorad) and bovine serum albumin for calibration.

NADHX dehydratase activity assays and thermostability testing

The NADHX dehydratase activity of purified recombinant wild-type and point-mutated cNAXD was assayed spectrophotometrically by monitoring S-NADHX consumption at 290 nm in a TECAN M200 Pro plate reader at 37°C. A reaction mixture (total assay volume of 200 µl) containing 25 mM HEPES, pH 7.1, 2 mM $MgCl_2$, 1 mM ATP, and various concentrations of S-NADHX was pre-incubated in UV-Star flat-bottom 96-well plates (Greiner Bio-One) in the plate reader until the signal was stable and the reaction was started by enzyme addition at a final concentration of 0.5 - 7.1 µg/ml. S-NADHX was synthesized and purified according to a protocol as described previously (Becker-Kettern *et al.*, 2018) and resuspended in 10 mM Tris, pH 8.0 prior to addition to the assay.

Kinetic constants of the NADHX dehydratase activity were determined in the presence of S-NADHX concentrations varying from 0 - 50 µM. The no substrate assays ([S-NADHX] = 0 µM) were used for background correction. For thermostability testing of the NAXD proteins, purified protein preparations (0.010—0.190 mg/ml depending on the preparation) were incubated at different temperatures (30—47°C) for 30 min prior to addition to the reaction mixture containing 10 µM S-NADHX and NADHX dehydratase activity assay at 37°C as described above.

Enzymatic activities were calculated using an extinction coefficient of 13,500 $M^{-1}cm^{-1}$ for S-NADHX as previously determined (Chaykin *et al.*, 1956) and a light path-length of 0.56 cm

(determined as recommended by the plate reader manufacturer). All measurements were done in at least three independent replicates and kinetic constants were obtained by fitting the values to a Michaelis-Menten regression using the GraphPad Prism Software (V7.02).

Metabolic stress assays

Fibroblast cells were seeded in basal media at 1 x 10^4 cells/ well into a 96-well dish and allowed to attach overnight. The following day media was replaced with either 100µL of DMEM (high-glucose, phenol-red free) supplemented with 10% fetal bovine serum (FBS), 2.05 mM L-glutamine, 100 units/mL penicillin, and 100 µg/mL streptomycin (basal medium) or 100µL of DMEM (glucose-free, phenol-red free) supplemented with 5mM galactose, 10% dialyzed FBS, 2.05 mM L-glutamine, 100 units/mL penicillin, and 100 µg/mL streptomycin (metabolic stress medium) and 50 µM sodium azide. Cell growth was monitored on a daily basis using the cell-permeable fluorescent dye Resazurin. At each time point, Resazurin (20µL/well of 0.15mg/ml solution) was added to each well and incubated at 37°C with 5% CO_2 for 4 hours prior to measuring relative fluorescent units (RFU; Ex=530-570 nm, Em=590-620 nm). Media-only values were subtracted from each reading on each day. RFU data at each time point was expressed relative to untreated cells on day 0. Growth rate was normalized its growth rate in basal medium to correct for intrinsic differences in absolute rates (Giordano *et al.*, 2014).

Immunoblotting

Cell proteins were extracted in RIPA buffer with gentle sonication (10 mM Tris-Cl (pH 8.0), 1 mM EDTA, 0.5 mM EGTA, 1% Triton X-100, 0.1% sodium deoxycholate, 0.1% SDS, 140 mM NaCl, 1mM PMSF and protease inhibitor cocktail (Roche)) and protein concentration determined with BCA assay (Pierce). SDS-PAGE was performed by loading equal amounts of protein (between 15- 25 µg of cell lysate per sample depending on the antibody used) using standard techniques on tris-glycine-SDS acrylamide gels (Biorad). Primary antibodies used were specific to NAXD (human CARKD Cat #ab82820, Abcam, human CARKD Cat #PA5-43038, Thermofisher and an antibody directed against a conserved region between human NAXD and mouse, CARKD, Cat #sc-514529 Santa Cruz Biotechnology) or mitochondrial respiratory chain subunits (mitochondrial OXPHOS antibody cocktail containing cytochrome *c* oxidase subunit 2 [COX2], cytochrome *b*-*c*1 complex subunit 2 [UQCRC2], succinate dehydrogenase [ubiquinone] flavoprotein subunit B [SDHB], NADH

dehydrogenase [ubiquinone] 1 beta subcomplex subunit 8 [NDUFB8] and ATP synthase subunit alpha [ATP5A]; Cat. #ab110411, Abcam). Porin detection (antibody Cat. #529534, Calbiochem) was used to normalize for mitochondrial density, and GAPDH detection (antibody Cat. #G9545) was used to normalize for total cellular protein. Primary antibodies were detected with anti-mouse or anti-rabbit horseradish peroxidase conjugated antibodies (GE Healthcare, NJ, USA), using enhanced chemiluminescence reagents (GE Healthcare, NJ, USA) and Amersham Hyperfilm. Protein band intensities were measured using ImageJ software, and band intensity determined in the linear range was normalized to band intensity of either porin or GAPDH.

OXPHOS enzyme activity assays

The complex I and complex IV dipstick activity assays were performed using 20 µg protein of whole cell lysates from control and subject fibroblasts following the manufacturer's instructions (catalogue numbers ab109720 and ab109876; MitoSciences, Eugene, OR, USA). The dipsticks were then placed in the MitoSciences MS1000 Dipstick Reader (MitoSciences, Eugene, OR, USA) for signal intensity quantitation. Data was normalized to protein concentration. Duplicate measurements were taken for each sample, and each cell line was assayed in triplicate.

Mitochondrial ROS production

Fibroblasts were seeded at $2x10^4$ cells/ well into 96-well black-walled, clear bottomed plates in basal media and allowed to attach overnight. The following day, the media was replaced with fresh basal media containing dihydroethidium (DHE, 10µg/ml) with or without rotenone (2.5µM). Cells were incubated at 37°C with 5% CO_2 for 45 minutes, washed with warm PBS, then 100 µl of warm PBS added to each well prior to DHE fluorescence being measured (Ex=320 nm, Em=615 nm, FLUOstar, BMG Labtech). PBS was then aspirated and replaced with 100 µl basal media containing Hoechst dye (2 µg/ml). The cells were incubated at 37°C with 5% CO_2 for 15 minutes, washed in warm PBS, then 100 µl of warm PBS was added to each well prior to measuring Hoechst fluorescence (Ex=340 nm, Em=460 nm). Relative fluorescent units (RFU) for DHE was normalized to the RFU for Hoechst for each well.

Lentiviral gene rescue

The coding sequences of mNAXD or cNAXD were PCR-amplified from the GenScript NAXD-pcDNA3.1 plasmid using primers containing flanking attB1 and attB2 sites and the PCR products were inserted into the Gateway pDONR221 vector as described above to generate the desired Entry vectors. The mNAXD and cNAXD inserts were then shuttled into the lentiviral destination vector pLX301 (pLX301 was a gift from David Root; Addgene plasmid # 25895 (Yang *et al.*, 2011)) using LR clonase, to generate the final NAXD-pLX301 constructs. The pLX301 unrecombined Destination vector is not suitable as a control construct as it contains the toxic CmR and ccdB genes. Therefore, a construct containing EGFP in the pLX301 lentiviral vector was generated to be used as a negative control. The EGFP-pLX301 control vector was generated by shuttling EGFP from the pDONR221_EGFP plasmid (a gift from David Root; Addgene plasmid # 25899 (Yang *et al.*, 2011)) into the pLX301 vector using LR clonase (Thermo Fisher Scientific). All vector identities were confirmed by Sanger sequencing. To generate lentiviral particles, human embryonic kidney (HEK) 293T cells at ~70% confluency on 10cm dishes were co-transfected in fresh basal medium with three plasmids (either mNAXD-pLX301 or cNAXD-pLX301 or EGFP-pLX301, the packaging plasmid pCMV-δ8.2, and the pseudotyping plasmid pCMV-VSVg used previously (Calvo *et al.*, 2012)) using Effectine reagents (Qiagen). Fresh medium was applied to the cells 16 hours after transfection, and after another 24 hours of incubation, media supernatants containing packaged virus were harvested and filtered through a 0.45 μm membrane. Primary human fibroblasts at a density of $3x10^5$ cells in triplicate 6-well dishes per construct were transfected with viral supernatant along with polybrene (5 mg/ml) (Sigma) for 48 hours. As a negative control, untransfected cells were treated with puromycin, to confirm puromycin sensitivity. As a positive control, untransfected cells at the same passage number were also expanded in parallel. Transfected cells were grown in antibiotic-free basal medium for 72 hours before application of basal medium containing puromycin (1 mg/ml) with daily media change for 7 days, then every 2-3 days for a further 9 days. After at least 16 days of selection, cells were expanded and harvested for NAD(P)HX metabolite analysis. All primers used for cloning and sequence verification are listed in Supplementary Table 2.

Statistical analysis

Statistical analyses were carried out using either a two-tailed student's t-test or one-way ANOVA corrected for multiple comparisons as appropriate (GraphPad Prism® Software).

Error bars represent the standard deviation of the mean (± SD). A p-value <0.05 was considered to be statistically significant.

Subject clinical summaries

Case 1 clinical summary

This previously healthy 3 year 7 month old boy was first admitted with a two week history of behavior change occurring after hitting his head on a glass table, without losing consciousness. His behavior worsened over the two week period. He had a history of delayed speech development but had stopped talking, dribbled, put objects in his mouth, clenched his fists, scratched his face, and made mumbling noises. In addition he had mild gait unsteadiness. The parents are non-consanguineous.

Apart from being clumsy no focal neurological deficit was noted. Investigations at that time including a full metabolic work up of blood, urine and CSF (including lactate) were normal except for detection of oligoclonal bands in cerebrospinal fluid (CSF). Initial brain Magnetic Resonance Imaging (MRI) and electroencephalography (EEG) were normal. He made some improvement during his hospital stay and was discharged without treatment.

He was readmitted two months later after further deterioration of gait, behavior and speech. As oligoclonal bands were still present in the CSF he was treated for autoimmune encephalitis with intravenous immunoglobulin and high dose intravenous methylprednisolone. Two months after his initial presentation he had an episode of pancytopenia. At that stage he had a very high C reactive protein of 225mg/L (normal up to 10). A bone marrow aspiration showed decreased granulopoiesis with markedly left shift with few mature neutrophils and an occasional precursor showing cytoplasmic vacuolation. There was markedly decreased erythropoietic activity represented by occasional early pro-erythroblasts. The majority of these pro-erythroblasts had cytoplasmic vacuolation. There were very occasional mature forms and some binucleate forms seen. Megakaryocytes were present and an increase in plasma cells was seen. There were plentiful iron stores with an occasional ring sideroblast seen in mature erythroid cells. The blood count gradually improved over the next month to normal without any specific treatment.

After discharge he had increased aggression, worsening ataxic gait and further deterioration in his speech which was by now completely lost. Three months later he developed “burn like” skin lesions in the groins and axillae. Repeat haematological, biochemical investigations and computed tomography (CT) of abdomen and pelvis were normal. Measles serology in blood and CSF was normal. A brain biopsy showed extensive neuronal damage and reactive gliosis. Liver and rectal biopsies were normal. He was started on biotin and thiamine. Around this

time he began having short seizures and was started on anti-epileptic drugs. EEGs showed epileptiform activity bilaterally. Choreiform movements and dystonia were noted.

Despite treatment he continued to deteriorate with bilateral ophthalmoplegia, spastic quadriplegia, and more prominent chorea and dystonia It later became apparent that he was deaf with profound bilateral sensorineural hearing loss. He continued to have seizures despite anti-epileptic drug therapy.

He was re-admitted at 4 years 6 months of age with fevers, mucositis, and vesicular lesions on his penis and anal area. These lesions were positive for herpes simplex virus. This was associated with profound pancytopenia. A bone marrow examination showed a markedly hypocellular bone marrow. Also in the course of this admission he developed a respiratory syncytial virus (RSV) infection and diarrhoea which resolved. He was started on granulocyte stimulating factor to which he initially responded well with improvement of his clinical condition. However the neutrophil count remained low after a brief improvement. He was discharged from the hospital but 4 days later became tachypnoeic and died soon after. Permission for autopsy was refused. Fibroblast cultures were established as part of the diagnostic investigations.

Case 1 MRI Scans

On the first admission the MRI scan was normal. Three months later it showed progression of disease with now bilateral, nearly symmetrical diffusion changes in the entire frontal lobes, as well as the anterior frontal lobes and the anterior temporal lobes with bilateral hippocampal involvement. Extensive diffusion abnormalities were also identified within the caudate head, globus pallidus bilaterally and thalamus. The lesions were T2 hyperintense (Fig. 1 A – C). Further MRI scan one month later showed diffusion restriction and increased T2 signal in the basal ganglia, grey matter and to a lesser extent adjacent to the subcortical white matter of the frontal parafalcine/surface gyri. M agnetic resonance angiography and venogram showed no vascular obstruction (Fig. 1 D – F). Three years later MRI showed marked diffuse bilateral cerebral atrophy, particularly in the frontal and anterior temporal lobes, associated with white matter volume loss and ex vacuo dilatation of the lateral and third ventricles. Bilateral deep and subcortical T2 and FLAIR hyperintensities of the cerebral white matter were most prominent in the frontoparietal and temporal lobes. In addition, there was marked hyperintensity, consistent with gliosis, within the frontal lobes bilaterally. The corpus callosum was diffusely thinned (Fig. 1 G – I). Inner ear structures were normal.

Case 1 Genetic Investigations

WES data from Case 1 revealed no rare homozygous variants, and two genes with rare compound heterozygous variants; NAD(P)HX Dehydratase (*NAXD*) and spectrin, beta, erythrocytic (*SPTB*). *SPTB* is linked to autosomal dominant type 2 spherocytosis, which is characterized by the presence of spherical-shaped erythrocytes (spherocytes) on a peripheral blood smear. Haematological investigations did not identify any morphological abnormalities in spherocytes in pre-transfusion blood films from the subject, providing no support that the identified *SPTB* compound heterozygous variants were likely to be disease-causing. Furthermore, variants in *SPTB* would not explain the neurological abnormalities observed in the subject. However, the compound heterozygous variants in *NAXD* (NM_001242882.1; c.839+1G>T, p.(?); c.922C>T, p.(Arg308Cys)) were considered to be of potential significance (Table 2, Supplementary Table 1 and Supplementary Fig. 1) because Case 1 shared many clinical features with NAXE deficient subjects, including episodes of fever and illness prior to deterioration, neurodegeneration and early death (Kremer *et al.*, 2016; Spiegel *et al.*, 2016). In addition, 51 heterozygous variants were identified in Case 1 by WES which were not considered pathogenic or validated at this stage. As Case 1 was a boy, X-linked analysis was also performed without any rare deleterious variants detected.

Case 1 Histological Investigations

Two skin punch biopsies from Case 1 showed an epidermis that had detached from the underlying dermis. There was extensive necrosis of the epidermis with lifting of the epidermis almost completely, with the separation being at the dermoepidermal junction just above the basement membrane. Some vacuolated basal cells were still present around the superficial hair follicle. There were a few inflammatory cells noted on one biopsy (scattered eosinophils and lymphocytes in the epidermis and in the subepidermal blister) with some inflammation in the dermis. The upper dermis was oedematous. The papillary dermis showed dilation of the superficial vessels and pigment incontinence, but no significant inflammation. The subcutis showed focal septal inglammantion and necrosis. There was no vasculitis and the biopsies were nevative for the following markers; C1q, C3C, IgM, IgG, IgA and fibrinogen. Overall

there was a subepidermal blistering skin presentation with extensive epidermal necrosis.

Case 1 Further Investigations

Whole body positron emission tomography (PET) and CT of abdomen and pelvis did not reveal any tumor. Extensive viral studies were normal. Metabolic investigations included urinary glycosaminoglycans, amino and organic acids, , white cell lysosomal enzyme assay, plasma very long chain fatty acids, transferrin isoforms, plasma and urine creatine and guanidinoacetate, biotinidase assays, heavy metals (copper, lead, selenium, zinc), porphyria assay, thyroid studies and antinuclear antibody and lupus studies, N-Methyl-D-aspartic acid or N-Methyl-D-aspartic acid receptor antibody assay and voltage gated potassium channel-complex antibody assays, CSF and serum lactate and liver function tests were all negative. A brain biopsy was PCR negative for *Herpes simplex*. The subject's karyotype was normal male, 46XY. Mitochondrial respiratory chain enzymology performed on a liver sample was all normal. Sequencing of the *POLG* gene was normal. Mitochondrial deletion and duplication studies were also normal.

Case 2 Clinical summary

Case 2 was the second child of healthy unrelated parents. She was born at full term in good condition with a birth weight of 3.8kg. She was healthy with normal development until age 14 months. At this age she was cruising but not yet walking independently and could say one or two words. She presented at age 14 months with progressive generalized dystonia, irritability, oral mucositis, diarrhoea and pancytopenia. Her condition improved slowly over several months with supportive treatment such that her dystonia resolved but she remained ataxic with axial hypotonia and ophthalmoplegia. She was unable to walk or speak but could finger feed and use a spoon. Over the following 2 years until her death at age 3 years and 10 months she suffered approximately 6 or 7 similar episodes of severe dystonia with further loss of skills after each. Fevers were associated with some, but not all episodes. In addition, there were more frequent episodes of pancytopenia accompanied by mucositis, vomiting, diarrhoea and skin rash. Brain MRI during the initial episode revealed bilateral hyperintensity of striatal nuclei and this remained unchanged in subsequent scans (Fig. 1 J – M). CSF analysis was normal and screening of blood, urine and CSF revealed no evidence of infection. Muscle biopsy showed changes compatible with neurogenic atrophy only and skin biopsy

showed epidermal necrosis with re-epithelialisation, vacuolar damage of the basal membrane and dermo-epidermal detachment. Bone marrow aspirate showed hypoplasia of all three cell lines, interstitial infiltrate (30-40%) and abundant stromal ferric deposits. Respiratory chain studies of biopsied muscle showed decreased activities of complexes II+III. Normal investigations included blood and urine amino acids, urine organic acids, CSF lactate, fibroblast pyruvate dehydrogenase activity, chromosome breakage studies (diepoxybutane, DEB) and echocardiogram. Sequencing of a panel of genes associated with defects in oxidative phosphorylation and with cyclic neutropenia as well as sequencing of the mitochondrial genome revealed no likely disease causing variants and there was no evidence of mitochondrial DNA depletion in muscle or bone marrow.

Case 2 Genetic Investigations

WES data from Case 2 and parental samples were analysed by trio analysis. Rare potentially deleterious variants were then selected by different modes of inheritance (*de novo*, homozygous and compound heterozygous). In Case 2, using MAF filters of <0.001, there were three genes identified with compound heterozygous variants, and only one likely heterozygous *de novo* SNV/indel variant (with balanced read depth). The compound heterozygous genes included *NAXD* (NM_001242882.1; c.187G>A, p.(Gly63Ser); c.948_949insTT, p.(Ala317Leufs*64)), *KIAA1586* (E3 SUMO-protein ligase) and *RECQL4* (ATP-dependent DNA helicase). *RECQL4* was not considered a likely candidate because it is associated with Baller-Gerold, Rothmund-Thomson and or RAPADILINO syndrome, which present with growth retardation and other features including skeletal abnormalities. In addition one of the variants was synonymous and the other predicted to be tolerated and not conserved. *KIAA1586* is not a known disease gene and the variants (an intronic duplication and a missense variant) were not likely to be deleterious. Therefore, *NAXD* was considered the most likely candidate gene (Table 2, Supplementary Table 1 and Supplementary Fig. 1). There was a heterozygous *de novo* SNV/indel variant in *TUFM* (mitochondrial Elongation Factor Tu) which was potentially interesting as recessive variants in this gene have been associated with combined oxidative phosphorylation deficiency resulting in severe lactic acidosis and a range of other symptoms including severe infantile macrocystic leukodystrophy (Valente *et al.*, 2007), encephalomyopathy or hypertrophic cardiomyopathy (Smeitink *et al.*, 2006). However, this was a heterozygous variant, with no evidence of a

second variant in trans, and CSF lactate levels were normal making this variant unlikely to be causative.

Case 3 Clinical summary

The 10-month-old female was second born to non-consanguineous parents at term by elective caesarean section. At birth, her weight was 2.5 kg (normal), length was 44 cm (-2.5 SD) and head circumference was 32.5 cm (normal). She had a female sibling who suddenly died. The female sibling was born by emergency caesarean section due to uncontrolled hypertension in the mother. The sibling had poor weight gain during infancy, mild developmental delay, mild anemia, recurrent episodes of fever and became lethargic at the age of 1 year 6 months. The sibling died after an episode of vomiting and lethargy at 1 year 7 months. In view of her sibling's unexplained death, a metabolic workup was carried out for Case 3 at a young age. On day 3, her blood lactate levels was 4.08 mmol/L (normal 0.5-1 mmol/L). The lactate levels at 2, 3, 4 and 6 months were 4.0, 8.8, 6.5 and 3.5 mmol/L respectively. Tandem mass spectrometry blood newborn screening returned normal metabolites, whereas urine gas chromatography–mass spectrometry showed elevated levels of lactic acid, succinic acid and 2-oxo-glutaric acid. Developmental milestones were normal for her age and she achieved sitting without support, monosyllables and stranger anxiety by 10 months. She had one episode of fever diagnosed as a urinary tract infection. She grew well and at 10 months her weight was 7.4 kg (normal), length was 69 cm (normal) and head circumference was normal. Her 2D-ECHO and MRI and MRS brain were reported normal.

The child was healthy till the age of one year when she had an episode of acute gastroenteritis. There were 2 - 3 episodes of vomiting followed by loose stools the following day. She was treated with anti-emetics and oral fluids and recovered. A week after this illness, her parents noted lethargy and a decreased appetite. She was admitted to hospital for observation. On clinical examination she had a normal heart rate, blood pressure and respiratory rate. Her tone was mildly decreased. The rest of the systemic examination was unremarkable.

She had mild anemia (Hb: 10.5 gm %) with microcystosis (MCV: 59.2 fl). Leucoytosis was noted with total leukocyte count of 19,900/ul. Liver enzymes were slightly elevated (ALT-107 IU/L, AST-156 IU/L). Blood glucose, renal function tests, ESR and CRP were within normal limits. Blood lactate was increased (37.5 mg/dl).

On day 2 of admission, she had an episode of vomiting, followed by uprolling of eyeballs, cyanosis and bradycardia. Resuscitative measures were initiated. However, she did not respond to these measures and succumbed.

The previous sibling of the proband was born at term by emergency caesarean section due to uncontrolled hypertension in mother. She weighed 2.4 kg (normal), length was 42.5 cm (-2.8 SD) and head circumference was 33 cm (normal). She had repeated febrile illnesses and poor weight gain during infancy. She could support her head against gravity by 3 months, roll over at 5 months and sat unaided at 9 months. She could walk with support at the age of 1 year 6 months. At this age she was mildly lethargic and not gaining weight. The tests performed were repeated at 11 months, with mild microcytic hypochromic anemia identified (Hb-8.7 gm/dl). She was treated with oral iron supplements. At 1 year 7 months she had lethargy and one episode of vomiting followed by sudden death. No other investigations were undertaken.

Case 3 Genetic Investigations

WES was performed for Case 3 and her parents. After data analysis of the trio, no *de-novo* or compound heterozygous variants of pathogenic significance were identified. However, a homozygous frameshift loss-of-function variant in *NAXD* was noted (NM_001242882.1; c.51_54delAGAA, p.(Ala20Phefs*9); Table 2, Supplementary Table 1 and Supplementary Fig. 1). This was considered a candidate variant due to the predicted crucial role of NAXD in mitochondrial function, evidence of persistent lactic acidosis in the proband and early unexplained sudden death in the previous sibling.

Case 4 Clinical summary

This boy, the first child to non-consanguineous White British parents, had normal development until 3 months of age at which time he was first admitted after an apparently trivial viral infection and regressed developmentally with the onset of infantile spasms and showed loss of previously attained skills such as visual attention, head control and social smiling. Within a week he also displayed explosive onset of infantile spasms with a hypsarrhythmic EEG and he was commenced on adrenocorticotropic hormone injections for these. MR imaging at that time demonstrated symmetrical high T1 changes in the basal

ganglia (globus pallidi and caudate) associated with restricted diffusion suggestive of a mitochondrial disorder (Fig. 1 N).

After 2 weeks of steroid treatment the child suffered an acute respiratory collapse and was noted to have extensive, progressive skin lesions in the form of a purple rash on the neck in both axillae and over the occiput, back and buttocks. He commenced antibiotic treatment for presumed cellulitis but given the unusual appearance of the skin, he proceeded to have a punch biopsy, which showed an acute, full thickness epidermal necrosis best classified as toxic epidermal necrolysis. No bacteria were identified on histology.

The child remained critically ill and developed a pancytopenia with a haemoglobin of 74g/L (normal range 105-122), platelets of 15 x 10^9/L (normal range 150-400) and leucopenia of 0.6 x 10^9/L (normal range 5.0-17.5). There was absolute neutropenia with the blood film showing no detectable neutrophils, crenated and diamorphic red cells and a few atypical lymphocytes. Bone marrow aspirate was haemodilute and showed limited haematopoiesis with evidence of increased macrophage activity with some vacuolated macrophages seen. Lymphocyte subset analysis demonstrated absent CD16+ NK cell [<0.01 x 10^9/L (normal range 0.1-1.3)], reduced CD3+ T-cells [0.58 x 10^9/L (normal range 2.3-6.5)] but preserved CD19+ B-Cells [0.99 x 10^9/L (normal range 0.6-3.0)]. Inflammatory markers were elevated with highest C-reactive protein 133 mg/L (normal range 0-10) and ferritin 438 µg/L (normal range 20-159). Ophthalmic examination demonstrated bilateral cataracts and echocardiography revealed left ventricular hypertrophy.

Despite intensive support, the child demonstrated no spontaneous respiratory drive and repeat MR imaging demonstrated extensive progression of the intracranial abnormalities. The basal ganglia and thalamic changes were more necrotic with multiple haemorrhagic foci and there was now involvement of the putamen bilaterally which were swollen with restricted diffusion. The brain was more oedematous generally, with patchy cortical and white matter oedema but with relative sparing of the post-central gyrus, occipital and temporal poles. There was widespread patchy restriction of diffusion in the cortex and white matter although the subcortical white matter appeared more affected than the deep white matter. The corticospinal tracts also showed restricted diffusion, extending down into the brain stem and both hippocampi were affected. There was oedema noted in the pons and medulla. The extra-axial CSF spaces and lateral ventricles were a little more prominent indicating a mild degree of cerebral atrophy. MR spectroscopy showed a lactate peak in the deep grey nuclei and in the cerebrum.

A muscle biopsy was taken for further mitochondrial investigations, following which critical care support was withdrawn with parental consent and the child died shortly afterwards.

Case 4 Genetic Investigations

Since Case 4 presented clinically with a suspected mitochondrial disorder, an initial gene panel of common nuclear Complex I genes revealed no abnormalities. Follow up investigations by WES trio analysis revealed a homozygous missense variant in *NAXD* (NM_001242882.1; c.308C>T, p.(Pro103Leu)) that was heterozygous in both parents (Supplementary Fig. 2). *In silico* analysis predicted the variant to be highly pathogenic, and the variant resided in a highly conserved residue (Table 2 and Supplementary Table 1).

Case 4 Further Investigations

Extensive viral studies were normal with no positive PCR result in CSF for CMV, HSV1, HSV2, HHV6, Parechovirus, VZV and Enterovirus. Blood PCR for CMV, EBV and Adenovirus was negative. Swabs of the skin lesions grew no organisms although oral swabs did grow *Candida albicans* and *Staphylococcus aureus* which were appropriately treated. Metabolic investigations included normal urinary glycosaminoglycans and organic acids. Urine amino acids and oligosaccharides demonstrated some interference from drug metabolites. Plasma very long chain fatty acids were essential normal with only an insignificant marginally low C24/C22 ratio. Biotinidase assay, acylcarnitines and total homocysteine was normal. CSF lactate was 2.1 mM. Muscle respiratory chain analysis demonstrated normal activities of complex IV and complexes II+III but decreased activity of complex I [ratio to citrate synthase 0.084 (normal range 0.104 - 0.268)]. The main abnormality on muscle histology was non-specific variability in fibre diameter. Given the profound neutropenia with cardiomyopathy, cardiolipin screening for Barth syndrome was performed which showed normal monolysocardiolipin/cardiolipin characteristics. Given the explosive onset of seizures CSF alpha-interferon was analysed for Aicardi-Goutieres Syndrome and this was <2.0 iU/L.

Case 5 Clinical summary

Case 5 was a healthy girl from Indian parents who was well until age 2 years 6 months when she was admitted with a two week history of intermittent vomiting, on a background of a longstanding history of frequent vomiting. Twenty-four hours before admission, she became unsteady on her feet and had intermittent jerky movements of all four limbs; these were occurring every few minutes by the time of admission. Her gait was unsteady and she was noted to be lethargic.

Investigations at her local hospital included a lumbar puncture, which showed no definitive evidence of infection. A CT brain scan was normal. She was given a presumed diagnosis of meningoencephalitis and commenced on antibiotics. She had a persistent tachycardia and was increasingly lethargic. An echocardiogram two days after admission showed evidence of a dilated cardiomyopathy, with severely impaired ventricular function (ejection fraction 17%). That same day, she rapidly deteriorated and became profoundly unwell with shallow respirations. She subsequently became apnoeic and pulseless, requiring cardiopulmonary resuscitation for six minutes. She was ventilated and transferred to a specialist cardiac unit on high inotropic support.

Investigations on admission revealed: high sodium, potassium and urea compatible with dehydration, glucose 11.6mmol/L; ALT and AST were raised, with normal ALP; raised random cortisol, but subsequently normal short synacthen test. The day after admission, she had a creatine kinase of 19,106 U/L (normal 25-146 U/L), amylase 235 U/L (normal 28-100 U/L), troponin 9,752 ng/L (normal 0-40) and BNP 2,874 ng/L (normal 0-40 ng/L).

Her echocardiogram showed poor biventricular function. She was treated with IV immunoglobulins, in case she had an acute myocarditis, and carnitine supplementation. Her ejection fraction on admission was 27%, with a fractional shortening of 12.5%. She made a fast clinical recovery and within four days she was extubated and was able to sit up and play with toys.

Further investigations were undertaken over the next two days. These revealed: normal lipase, essentially normal plasma acyl carnitines but with mildly raised hexanoyl and octanoyl carnitines, mild iron deficiency anaemia; high initial serum urate that rapidly returned to normal. The folate and vitamin B12 were high; normal plasma amino acids. A viral screen revealed evidence of previous, not current Coxsackie A infection. Her maximum CRP was 21mg/L. Immunoglobulins were normal, whilst complement C3 and C4 were marginally low. The blood ammonia was normal, and high initial blood lactate normalized on recovery. Vitamin D was low (15nmol/L; >50 – 75 nmol/L adequate; >75nmol/L optimal). Ultrasound of her abdomen and pelvis were normal, except for some free fluid. A primary

carnitine deficiency was suspected in view of the high initial creatine kinase and amylase in the presence of a severe dilated cardiomyopathy. However, *SLC22A5* mutation analysis was normal.

She was well for the next two months, and despite having an episode of vomiting and an upper respiratory tract infection, she had not decompensated. Her ejection fraction when well was 62%.

She was then however readmitted following a 24-hour history of vomiting with evidence of an *E. coli* confirmed urinary tract infection. A repeat echocardiogram was performed within 24 hours of admission and showed an ejection fraction of 12%. She rapidly deteriorated, requiring ventilation, and was readmitted to the cardiac intensive care unit. Her lactate was high (15mmol/L; nomal range <0.5 - 1 mmol/L). She was commenced on high dose inotropic support. Due to rapid worsening of her cardio-respiratory status, she required extracorporeal membrane oxygenation (ECMO). Her clinical condition improved rapidly and she was weaned off the ECMO after two days; five days after admission, her cardiac function had again normalized.

A muscle biopsy was performed during that admission which showed an abnormal population of scattered very small fibers expressing fetal developmental myosin chain isoforms. Muscle fibres showed increased coarse oxidative staining in a mosaic distribution with retained COX positive ragged red equivalents. There was a mild to moderate diffuse increase in lipid staining. Immunostaining by *TOMM20* did not suggest any depletion of complex 1 and IV subunits. Skeletal muscle EMG of the tibialis anterior suggested a myopathic process.

Brain MRI showed symmetrical bilateral abnormal white matter signal in the frontal lobes with some overlying thinning of the cortex. Focal changes were also seen in the left tempero-occipital and left parietal lobe. Notably, there was no abnormal signal in the basal ganglia.

She remained well upon discharge, but two months later, she was once again admitted in severe cardiac failure with rapid deterioration, after several days of vomiting and coryzal symptoms at home. ECMO was again commenced. It was not possible to wean her from the ECMO and treatment was withdrawn six days after this admission, with rapid demise. A full post-mortem was performed, but no other abnormalities that had not been detected prior to death were identified.

A dilated cardiomyopathy genetic panel including 59 genes was performed, but no pathogenic or likely pathogenic mutation was identified. The mitochondrial genome was fully sequenced and again no abnormality was identified.

Her development, up until her first admission, had not caused her parents any concerns; she was less energetic than her older brother aged four and except for her recurrent, almost nightly vomiting between seven and fifteen months of age, her parents were not concerned about her physical or cognitive development.

Her parents were non consanguineous, but from the same region in India. Their first child was born in Northern Europe and they returned to India when she was one year old. At thirteen months she was taken to the local GP with an episode of pallor and floppiness, following a vomit. It was noted that her heart beat was irregular and she was referred to hospital. She was admitted to intensive care, as she was extremely unwell. She was ventilated, but had a cardiac arrest within four hours of admission and resuscitation was unsuccessful. It was presumed that she had died of overwhelming sepsis. She had been previously well, although like her sister vomited frequently. Her brother remains fit and well. He does not vomit frequently and has more energy than either of his sisters. His cardiac screening has been normal.

Her parents have had normal cardiac investigations. The father, aged forty-two, has had five possible seizures, between the ages of sixteen and thirty-two years, associated with periods of stress, such as 'overworking' and 'sleep deprivation'. He took anti-epileptic medication for three years and then stopped and has not had any further episodes over the last ten years. His MRI brain was normal.

The Guthrie card from the first child also showed the homozygous mutation in *NAXD* that was found in his affected sister, whilst the youngest brother is heterozygous, as are both parents. Fibroblast cultures failed to establish from a skin biopsy.

Case 5 Genetic Investigations

The WES data generated for Case 5 was analysed using the same methodology as for Case 2. A homozygous variant was identified in *NAXD* (NM_001242882.1; c.54_57delAAGA, p.(Ala20Phefs*9)) that was heterozygous in both parents. The *NAXD* variant appeared likely a strong candidate as it was predicted to be pathogenic, leading to a frameshift and early truncation of the protein.

Case 6 Clinical summary

Case 6 was a child of non-consanguineous parents of German origin. She was occasionally hospitalized with an unknown bowel disease, balance problems, developmental delay, and

seizures with normal EEG and MRI reports. At 8 months of age, she presented with impaired coordination and delay of motor abilities. At the age of one year and seven months she was taken to the hospital after a seizure-like event (right sided hemiplegia, right hand flexion and jerks). She had fever and showed elevated inflammation parameters. During the hospitalization EEG and MRI showed a rapid deterioration with increased signal intensity in the frontal cortical region as well as in the caudate nucleus and putamen. Moreover, frontal brain oedema was seen bilaterally. She showed general developmental regression: she lost her ability to sit, to hold her head upright, and eventually did not show any spontaneous motor activity apart from occasional alternating eye and hand movements. Skin manifestations consisting of redness, blistering and peeling were observed in the anogenital region and on the proximal phalanges of the 4th and 5th finger of the right hand. Gastrointestinal imaging discovered focal erythematous and partly aphthous insular lesions. A metabolic disorder was suspected but investigations for metabolic abnormalities, including muscle biopsy, were inconclusive. Muscle respiratory chain analysis demonstrated normal activities of Complex II+III but reduced activity of Complex I [ratio to citrate synthase 0.07 (normal range 0.17 - 0.56)] and Complex IV [ratio to citrate synthethase 0.65 (normal range 1.10 – 5.00)]. After a rapid regression, at the age of 22 months, the young girl passed away.

Case 6 Genetic Investigations

WES data from Case 6 was analyzed using methods as previously described (Kremer *et al.*, 2017) and as detailed in Supplementary Materials. Filtering for genes harboring bi-allelic variants with a minor allele frequency (MAF) of less than 1% using the Munich in-house database consisting of 14,000 exomes revealed 7 candidate genes. However, none of these genes was reported to be associated with a mitochondrial disorder or encode for a mitochondrial protein, nor did the genes harbor predicted loss-of-function variants. Due to this inconclusive analysis, trio-analysis was performed to search for *de novo* variants. The search identified 3 genes harboring one missense variant, each of which was exclusively detected in the subject but not the parents. Two of these variants were predicted probably damaging, one of them residing in the mitochondrial protein encoding gene *NAXD* (NM_001242882.1; c.331C>T, p.(Leu111Phe); Table 2, Supplementary Table 1 and Supplementary Fig. 1). Strikingly, the subject's phenotype closely resembled the clinical presentation of subjects carrying pathogenic bi-allelic variants in *NAXE* (Kremer *et al.*, 2016). To clarify whether the identified variant acted in a dominant fashion or the variant was

compounded by a second coding or non-coding heterozygous variant, WGS was performed (Kremer *et al.*, 2017). There was no rare (MAF <1%) non-coding variant in *NAXD* but we identified a second *de novo* missense variant, predicted as possibly damaging which was only present in 18% of the reads (NM_001242882.1; c.776T>G, p.(Leu259Arg); Table 2, Supplementary Table 1, Supplementary Fig.s 1 and 2). This variant was also detectable upon re-analysis of the exome data in 16% of the reads and so was discarded in the initial analysis. Importantly, no other individual in the Munich in-house database carried rare (MAF <1%) predicted damaging bi-allelic variants in *NAXD*.

Additional references

Adzhubei IA, Schmidt S, Peshkin L, Ramensky VE, Gerasimova A, Bork P, *et al.* A method and server for predicting damaging missense mutations. Nat Methods 2010; 7(4): 248-9.

Becker-Kettern J, Paczia N, Conrotte J-F, Zhu C, Fiehn O, Jung PP, *et al.* NAD(P)HX repair deficiency causes central metabolic perturbations in yeast and human cells. bioRxiv 2018.

Calvo SE, Compton AG, Hershman SG, Lim SC, Lieber DS, Tucker EJ, *et al.* Molecular diagnosis of infantile mitochondrial disease with targeted next-generation sequencing. Sci Transl Med 2012; 4(118): 118ra10.

Chaykin S, Meinhart JO, Krebs EG. Isolation and properties of a reduced diphosphopyridine nucleotide derivative. J Biol Chem 1956; 220(2): 811-20.

Cooper GM, Stone EA, Asimenos G, Program NCS, Green ED, Batzoglou S, *et al.* Distribution and intensity of constraint in mammalian genomic sequence. Genome Res 2005; 15(7): 901-13.

Danecek P, Auton A, Abecasis G, Albers CA, Banks E, DePristo MA, *et al.* The variant call format and VCFtools. Bioinformatics 2011; 27(15): 2156-8.

Genomes Project C, Auton A, Brooks LD, Durbin RM, Garrison EP, Kang HM, *et al.* A global reference for human genetic variation. Nature 2015; 526(7571): 68-74.

Giordano C, Iommarini L, Giordano L, Maresca A, Pisano A, Valentino ML, *et al.* Efficient mitochondrial biogenesis drives incomplete penetrance in Leber's hereditary optic neuropathy. Brain 2014; 137(Pt 2): 335-53.

Girisha KM, Shukla A, Trujillano D, Bhavani GS, Hebbar M, Kadavigere R, *et al.* A homozygous nonsense variant in IFT52 is associated with a human skeletal ciliopathy. Clin Genet 2016; 90(6): 536-9.

Guo Y, Ding X, Shen Y, Lyon GJ, Wang K. SeqMule: automated pipeline for analysis of human exome/genome sequencing data. Sci Rep 2015; 5: 14283.

Kremer LS, Bader DM, Mertes C, Kopajtich R, Pichler G, Iuso A, *et al.* Genetic diagnosis of Mendelian disorders via RNA sequencing. Nat Commun 2017; 8: 15824.

Kremer LS, Danhauser K, Herebian D, Petkovic Ramadza D, Piekutowska-Abramczuk D, Seibt A, *et al.* NAXE Mutations Disrupt the Cellular NAD(P)HX Repair System and Cause a Lethal Neurometabolic Disorder of Early Childhood. Am J Hum Genet 2016; 99(4): 894-902.

Kumar P, Henikoff S, Ng PC. Predicting the effects of coding non-synonymous variants on protein function using the SIFT algorithm. Nat Protoc 2009; 4(7): 1073-81.

Lek M, Karczewski KJ, Minikel EV, Samocha KE, Banks E, Fennell T, *et al.* Analysis of protein-coding genetic variation in 60,706 humans. Nature 2016; 536(7616): 285-91.

Marbaix AY, Noel G, Detroux AM, Vertommen D, Van Schaftingen E, Linster CL. Extremely conserved ATP- or ADP-dependent enzymatic system for nicotinamide nucleotide repair. J Biol Chem 2011; 286(48): 41246-52.

Marbaix AY, Tyteca D, Niehaus TD, Hanson AD, Linster CL, Van Schaftingen E. Occurrence and subcellular distribution of the NADPHX repair system in mammals. Biochem J 2014; 460(1): 49-58.

Patiny L, Borel A. ChemCalc: A Building Block for Tomorrow's Chemical Infrastructure. Journal of Chemical Information and Modeling 2013; 53(5): 1223-8.

Philippakis AA, Azzariti DR, Beltran S, Brookes AJ, Brownstein CA, Brudno M, *et al.* The Matchmaker Exchange: a platform for rare disease gene discovery. Hum Mutat 2015; 36(10): 915-21.

Plagnol V, Curtis J, Epstein M, Mok KY, Stebbings E, Grigoriadou S, *et al.* A robust model for read count data in exome sequencing experiments and implications for copy number variant calling. Bioinformatics 2012; 28(21): 2747-54.

Richards S, Aziz N, Bale S, Bick D, Das S, Gastier-Foster J, *et al.* Standards and guidelines for the interpretation of sequence variants: a joint consensus recommendation of the American College of Medical Genetics and Genomics and the Association for Molecular Pathology. Genet Med 2015; 17(5): 405-24.

Smeitink JA, Elpeleg O, Antonicka H, Diepstra H, Saada A, Smits P, *et al.* Distinct clinical phenotypes associated with a mutation in the mitochondrial translation elongation factor EFTs. Am J Hum Genet 2006; 79(5): 869-77.

Spiegel R, Shaag A, Shalev S, Elpeleg O. Homozygous mutation in the APOA1BP is associated with a lethal infantile leukoencephalopathy. Neurogenetics 2016; 17(3): 187-90.

Stenson PD, Mort M, Ball EV, Howells K, Philips AD, Thomas NS, *et al.* The Human Gene Mutation Database: 2008 update. . Genome Med 2009; 1(13).

Valente L, Tiranti V, Marsano RM, Malfatti E, Fernandez-Vizarra E, Donnini C, *et al.* Infantile encephalopathy and defective mitochondrial DNA translation in patients with mutations of mitochondrial elongation factors EFG1 and EFTu. Am J Hum Genet 2007; 80(1): 44-58.

Wang K, Li M, Hakonarson H. ANNOVAR: functional annotation of genetic variants from high-throughput sequencing data. Nucleic Acids Res 2010; 38(16): e164.

Yang X, Boehm JS, Yang X, Salehi-Ashtiani K, Hao T, Shen Y, *et al.* A public genome-scale lentiviral expression library of human ORFs. Nat Methods 2011; 8(8): 659-61.

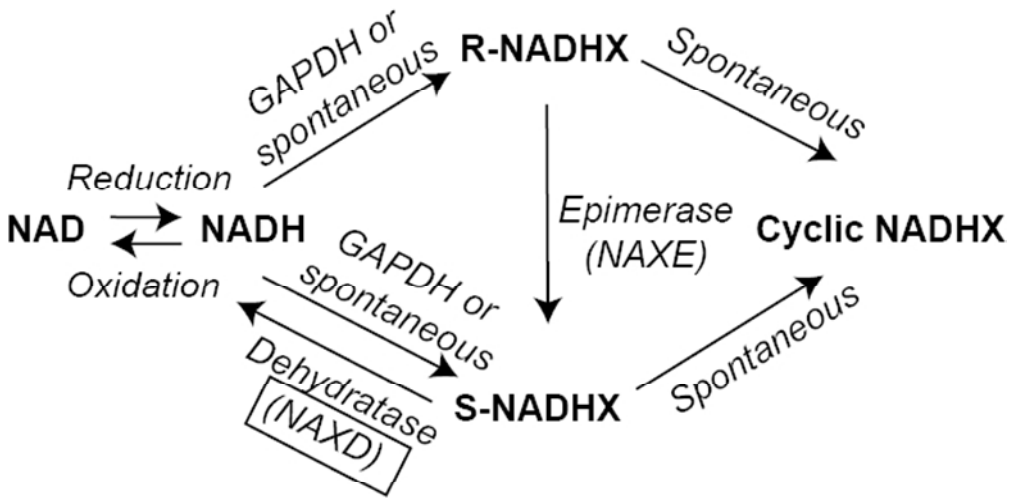

114x67mm (150 x 150 DPI)